RESEARCH ARTICLE

Detecting epistasis with the marginal epistasis test in genetic mapping studies of quantitative traits

Lorin Crawford[1,2,3]*, Ping Zeng[4,5], Sayan Mukherjee[6,7,8,9], Xiang Zhou[4,5]*

1 Department of Biostatistics, Brown University, Providence, Rhode Island, United States of America,
2 Center for Statistical Sciences, Brown University, Providence, Rhode Island, United States of America,
3 Center for Computational Molecular Biology, Brown University, Providence, Rhode Island, United States of America, **4** Department of Biostatistics, University of Michigan, Ann Arbor, Michigan, United States of America, **5** Center for Statistical Genetics, University of Michigan, Ann Arbor, Michigan, United States of America, **6** Department of Statistical Science, Duke University, Durham, North Carolina, United States of America, **7** Department of Computer Science, Duke University, Durham, North Carolina, United States of America, **8** Department of Mathematics, Duke University, Durham, North Carolina, United States of America, **9** Department of Bioinformatics & Biostatistics, Duke University, Durham, North Carolina, United States of America

* lorin_crawford@brown.edu (LC); xzhousph@umich.edu (XZ)

Abstract

Epistasis, commonly defined as the interaction between multiple genes, is an important genetic component underlying phenotypic variation. Many statistical methods have been developed to model and identify epistatic interactions between genetic variants. However, because of the large combinatorial search space of interactions, most epistasis mapping methods face enormous computational challenges and often suffer from low statistical power due to multiple test correction. Here, we present a novel, alternative strategy for mapping epistasis: instead of directly identifying individual pairwise or higher-order interactions, we focus on mapping variants that have non-zero *marginal epistatic effects*—the combined pairwise interaction effects between a given variant and all other variants. By testing marginal epistatic effects, we can identify candidate variants that are involved in epistasis without the need to identify the exact partners with which the variants interact, thus potentially alleviating much of the statistical and computational burden associated with standard epistatic mapping procedures. Our method is based on a variance component model, and relies on a recently developed variance component estimation method for efficient parameter inference and p-value computation. We refer to our method as the "MArginal ePIstasis Test", or MAPIT. With simulations, we show how MAPIT can be used to estimate and test marginal epistatic effects, produce calibrated test statistics under the null, and facilitate the detection of pairwise epistatic interactions. We further illustrate the benefits of MAPIT in a QTL mapping study by analyzing the gene expression data of over 400 individuals from the GEUVADIS consortium.

Author summary

Epistasis is an important genetic component that underlies phenotypic variation and is also a key mechanism that accounts for missing heritability. Identifying epistatic interactions in genetic association studies can help us better understand the genetic architecture of complex traits and diseases. However, the ability to identify epistatic interactions in practice faces important statistical and computational challenges. Standard statistical methods scan through all-pairs (or all high-orders) of interactions, and the large number of interaction combinations results in slow computation time and low statistical power. We propose an alternative mapping strategy and a new variance component method for identifying epistasis. Our method examines one variant at a time, and estimates and tests its *marginal epistatic effect*—the combined pairwise interaction effects between a given variant and all other variants. By testing for marginal epistatic effects, we can identify variants that are involved in epistasis without the need of explicitly searching for interactions. Our method also relies on a recently developed variance component estimation method for efficient and robust parameter inference, and accurate p-value computation. We illustrate the benefits of our method using simulations and real data applications.

Introduction

Genetic mapping studies, in the form of genome-wide association studies (GWASs) [1] and molecular trait quantitative trait loci (QTL) mapping studies [2–5], have identified thousands of genetic loci associated with many complex traits and common diseases, providing insights into the genetic basis of phenotypic variation. Most of these existing genetic mapping studies look at one variant at a time and focus on identifying marginal genetic associations that exhibit either additive or dominant effects. However, it has long been hypothesized that effects beyond additivity could contribute to a large proportion of phenotypic variation. In particular, epistasis—the interaction between genetic loci—is thought to play a key role in defining the genetic architecture underlying complex traits [6, 7] and constituting the genetic basis of evolution [8, 9]. Indeed, studies have detected pervasive epistasis in many model organisms [10–33]. However, substantial controversies remain [34–36]. For example, in some settings, genetic mapping studies have identified many candidates of epistatic interactions that contribute to quantitative traits and diseases [37–40], but some of these effects can be explained by additive effects of other unsequenced variants [41]. On the other hand, while previous variance partition studies have shown that genetic variance for many traits are mainly additive [34, 35, 42], these conclusions have been challenged recently [36]. Furthermore, while modeling epistasis has been recently shown to increase phenotype prediction accuracy in modal organisms [43] and facilitate genomic selection in animal breeding programs [44, 45], such conclusions do not hold in all settings [46]. Finally, epistasis has been recently proposed as one of the main factors that explain missing heritability—the proportion of heritability not explained by the top associated variants in GWASs [1, 47]. In particular, studies have hypothesized that epistasis can confound heritability estimation in pedigree studies and cause inflation of heritability estimates, creating the so-called "phantom heritability" [48, 49]. However, for some traits, the contribution of epistasis to missing heritability is negligible [50].

Nevertheless, because of the potential importance of epistasis in defining the genetic architecture of complex traits, many statistical methods have been developed to identify epistatic interactions in genetic mapping studies [51, 52]. Different existing statistical methods differ in their ways of selecting a testing unit (i.e. variants or genes [53]), their searching strategy (e.g.

exhaustive search [54–56] or probabilistic search [57] or prioritization based on a candidate set [58]), and the calculation of test statistics (e.g. various frequentist tests [59] or Bayesian approaches [60–62]). However, almost all of these statistical methods focus on explicitly searching for pairwise or higher-order interactions when identifying epistatic effects. Because of the extremely large search space (e.g. $p(p-1)/2$ pairwise combinations for p variants), these methods often suffer from heavy computational burden and low statistical power. Despite various efficient computational implementations [56, 63] and recently developed efficient search algorithms [57], exploring over a large combinatorial search space remains a daunting task for large epistasis mapping studies. Statistically, because of a lack of *a priori* knowledge of epistatic loci, exploring all combinations of genetic variants could result in low statistical power—on the other hand, restricting to a subset of prioritized combinations based on prior knowledge or marginal effects could also miss important genetic interactions.

Here, we present an alternative strategy for mapping epistasis. Instead of directly identifying individual pairwise or higher-order interactions, we focus on identifying variants that have a non-zero interaction effect with any other variants. To do so, we develop a novel statistical method, which we refer to as the the "MArginal ePIstasis Test" (MAPIT), to test each variant in turn on its *marginal epistatic effect*—the combined pairwise interaction effects between a given variant and all other variants. By testing marginal epistatic effects, we can identify candidate markers that are involved in epistasis without the need to identify the exact partners with which the variants interact—thus, potentially alleviating much of the statistical and computational burden associated with standard epistatic mapping methods. In addition, evidence of marginal epistasis can be used to further prioritize the search and identification of pairwise interactions. Our method is based on variance component models [64–76]. By taking advantage of a recently developed variance component estimation method [77] for efficient parameter inference and p-value computation, our method is scalable to moderately sized genetic mapping studies. We illustrate how MAPIT can serve as a useful alternative to standard methods in mapping epistasis with both simulations and a real data application.

Materials and methods

MAPIT model

We describe the MArginal ePIstasis Test in detail here. Our goal is to identify variants that interact with other variants, and to avoid explicitly searching for pairwise interactions. Therefore, unlike standard tests for epistasis, MAPIT works by examining one variant at a time. For the kth variant, we consider the following linear model,

$$\mathbf{y} = \mu + \mathbf{x}_k \beta_k + \sum_{l \neq k} \mathbf{x}_l \beta_l + \sum_{l \neq k} (\mathbf{x}_k \circ \mathbf{x}_l) \alpha_l + \boldsymbol{\varepsilon}, \quad \boldsymbol{\varepsilon} \sim \text{MVN}(\mathbf{0}, \tau^2 \mathbf{I}), \tag{1}$$

where $\mathbf{y}$ is an n-vector of phenotypes for n individuals; μ is an intercept term; $\mathbf{x}_k$ is an n-dimensional genotype vector for the kth variant that is the focus of the model; β_k is the corresponding additive effect size; $\mathbf{x}_l$ is an n-dimensional genotype vector for the lth variant, and l represents any of the p variants other than the kth; β_l is the corresponding additive effect size; $\mathbf{x}_k \circ \mathbf{x}_l$ denotes an element-wise multiplication between genotype vectors, thus representing the interaction term between the kth and l^{th} variants; α_l is the corresponding interaction effect size; $\boldsymbol{\varepsilon}$ is an n-vector of residual errors; τ^2 is the residual error variance; $\mathbf{I}$ is the identity matrix; and MVN denotes a multivariate normal distribution. In addition, we assume that the genotype vector for each variant has been centered and standardized to have mean 0 and standard deviation 1.

The model in Eq (1) is an underdetermined linear system ($p > n$). Therefore, we have to make additional modeling assumptions on the effect sizes β_l and α_l to make the model identifiable. To do so, we follow standard approaches [64, 67, 69] and assume that each individual effect size follows a normal distribution, or $\beta_l \sim N(0, \omega^2/(p-1))$ and $\alpha_l \sim N(0, \sigma^2/(p-1))$ for $l \neq k$. With the normal assumption on effect sizes, the model in Eq (1) is equivalent to the following variance component model,

$$\mathbf{y} = \mu + \mathbf{x}_k\beta_k + \mathbf{m}_k + \mathbf{g}_k + \boldsymbol{\varepsilon}, \quad \boldsymbol{\varepsilon} \sim \text{MVN}(\mathbf{0}, \tau^2\mathbf{I}), \tag{2}$$

where $\mathbf{m}_k = \sum_{l \neq k} \mathbf{x}_l\beta_l$ is the combined additive effects from all other variants, and effectively represents the additive effect of the kth variant under the polygenic background of all other variants; $\mathbf{m}_k \sim \text{MVN}(0, \omega^2 \mathbf{K}_k)$ with $\mathbf{K}_k = \mathbf{X}_{-k}\mathbf{X}_{-k}^{\mathsf{T}}/(p-1)$ being the genetic relatedness matrix computed using genotypes from all variants other than the kth; $\mathbf{g}_k = \sum_{l \neq k}(\mathbf{x}_k \circ \mathbf{x}_l)\alpha_l$ is the summation of all pairwise interaction effects between the kth variant and all other variants; and $\mathbf{g}_k \sim \text{MVN}(0, \sigma^2 \mathbf{G}_k)$ with $\mathbf{G}_k = \mathbf{D}_k \mathbf{K}_k \mathbf{D}_k$ representing a relatedness matrix computed based on pairwise interaction terms between the kth variant and all other variants. Here, we denote $\mathbf{D}_k = \text{diag}(\mathbf{x}_k)$ to be an $n \times n$ diagonal matrix with the genotype vector $\mathbf{x}_k$ as its diagonal elements. It is important to note that both $\mathbf{K}_k$ and $\mathbf{G}_k$ change with every new marker k that is considered.

We want to point out that the formulation of MAPIT in Eq (2) can also be easily extended to accommodate other fixed effects (e.g. age, sex, or genotype principal components), as well as other random effects terms that can be used to account for sample non-independence due to other genetic or common environmental factors. In addition, we choose to model β_k as a fixed effect here, but modeling it as a random effect is straightforward. Also note that, in this work, we limit ourselves to only consider second order epistatic relationships between SNPs. However, the generalization of MAPIT to detect higher order interactions is straightforward and only involves the manipulation of $\mathbf{G}_k$.

Point estimates

Our goal is to identify variants that have non-zero interaction effects with any other variant. To do so, we can examine each variant in turn ($k = 1, \ldots, p$) and test the null hypothesis in Eq (1) that variant k has no interaction effect with any other variant, $H_0 : \alpha'_l = 0 \ \forall \ l \neq k$. This same null hypothesis is specified in the variance component model stated in Eq (2) as $H_0 : \sigma^2 = 0$. The variance component σ^2 effectively captures the total epistatic interaction effects between the kth variant and all other variants—we call this the marginal epistatic effect for the kth variant.

Testing the marginal epistatic effect σ^2 requires jointly estimating the variance component parameters ($\omega^2, \sigma^2, \tau^2$) in Eq (2). The standard method for variance component estimation is the restricted maximum likelihood estimation (REML) method. However, REML is computationally slow: it requires an iterative optimization procedure where the time complexity of each iteration scales cubically with the number of individuals [66, 68–73]. The slow computation speed of REML is further exacerbated by the fact that the variance component model changes for every variant k (i.e. both $\mathbf{K}_k$ and $\mathbf{G}_k$ are variant specific)—hence, the variance component parameters are required to be estimated over and over again across genome-wide variants. Therefore, we cannot use REML for marginal epistatic mapping. Instead, we follow the recently developed MQS method [77] for efficient variance component estimation and testing. MQS is based on the method of moments and produces estimates that are mathematically identical to the Haseman-Elston (HE) cross-product regression [78]. Note that MQS is not only computationally more efficient than HE regression, but also provides a simple, analytic estimation form that allows for exact p-value computation—thus alleviating the need for

jackknife re-sampling procedures [79] that both are computationally expensive and rely on incorrect individual independence assumptions [80].

To estimate the variance components with MQS, we first multiply a projection matrix $\mathbf{M}_k$ on both sides of the model in Eq (2) to remove the influence of μ and $\mathbf{x}_k$. Here, $\mathbf{M}_k = \mathbf{I} - \mathbf{b}_k(\mathbf{b}_k^{\mathsf{T}}\mathbf{b}_k)^{-1}\mathbf{b}_k^{\mathsf{T}}$, where $\mathbf{b}_k = [\mathbf{1}_n, \mathbf{x}_k]$ with $\mathbf{1}_n$ denoting an n-vector of ones. Thus, $\mathbf{M}_k$ is a variant specific projection matrix onto both the null space of the intercept and the corresponding genotypic vector $\mathbf{x}_k$. By multiplying $\mathbf{M}_k$, we obtain the following simplified modeling specification

$$\mathbf{y}_k^* = \mathbf{m}_k^* + \mathbf{g}_k^* + \boldsymbol{\varepsilon}_k^*, \quad \mathbf{m}_k^* \sim \mathrm{MVN}(\mathbf{0}, \omega^2\mathbf{K}_k^*), \quad \mathbf{g}_k^* \sim \mathrm{MVN}(\mathbf{0}, \sigma^2\mathbf{G}_k^*), \quad \boldsymbol{\varepsilon}_k^* \sim \mathrm{MVN}(\mathbf{0}, \tau^2\mathbf{M}_k), \quad (3)$$

where $\mathbf{y}_k^* = \mathbf{M}_k\mathbf{y}$; $\mathbf{m}_k^* = \mathbf{M}_k\mathbf{m}$; $\mathbf{K}_k^* = \mathbf{M}_k\mathbf{K}_k\mathbf{M}_k$; $\mathbf{g}_k^* = \mathbf{M}_k\mathbf{g}$; $\mathbf{G}_k^* = \mathbf{M}_k\mathbf{G}_k\mathbf{M}_k$; and $\boldsymbol{\varepsilon}_k^* = \mathbf{M}_k\boldsymbol{\varepsilon}$, respectively. Note that Eq (3) also changes with every new marker k that is considered.

To simplify notation, we use $\boldsymbol{\delta} = (\omega^2, \sigma^2, \tau^2)$ to denote the variance components. Next, we use the notation $\sum_k = [\sum_{k,1}, \sum_{k,2}, \sum_{k,3}] = [\mathbf{K}_k^*, \mathbf{G}_k^*, \mathbf{M}_k]$. Lastly, we use indices $i, j, l \in \{1, 2, 3\}$ to represent the corresponding variance component or covariance matrix. Given estimates $\hat{\sum}_k$, we can obtain the MQS estimates for the variance components of each variant $(\hat{\delta}_{k,1}, \hat{\delta}_{k,2}, \hat{\delta}_{k,3}) = (\hat{\omega}_k^2, \hat{\sigma}_k^2, \hat{\tau}_k^2)$ via the following simple analytic formula

$$\hat{\delta}_{k,i} = \mathbf{y}_k^{*\mathsf{T}}\mathbf{H}_{k,i}\mathbf{y}_k^*. \qquad (4)$$

Here, we define $\mathbf{H}_{k,i} = (\mathbf{S}_k^{-1})_{ii}\hat{\sum}_{k,i} + (\mathbf{S}_k^{-1})_{ij}\hat{\sum}_{k,j} + (\mathbf{S}_k^{-1})_{il}\hat{\sum}_{k,l}$, where $\mathbf{S}_k$ is a 3×3 matrix in which $\mathbf{S}_{k,ij} = \mathrm{trace}(\hat{\sum}_{k,i}\hat{\sum}_{k,j})$ for every $i, j, l = 1, 2, 3$.

Hypothesis testing

MAPIT provides two options to compute p-values. The first option is approximate, and is based on a normal test that only requires the variance component estimate $\hat{\sigma}^2$ and its corresponding standard error. In particular, the variances of the MQS estimates in Eq (4) are given via a previously suggested and computationally efficient approximation [77]

$$\mathrm{V}(\hat{\delta}_{k,i}) \approx 2\mathbf{y}_k^{*\mathsf{T}}\mathbf{H}_{k,i}^{\mathsf{T}}\mathbf{V}_k\mathbf{H}_{k,i}\mathbf{y}_k^*, \qquad (5)$$

where $\mathbf{V}_k = \hat{\omega}_k^2\mathbf{K}_k^* + \hat{\sigma}_k^2\mathbf{G}_k^* + \hat{\tau}_k^2\mathbf{M}_k$. Given an estimate from Eq (4) and its standard error from Eq (5), we can perform a normal test (or z-test) to compute p-values. More specifically, we use a two sided test since the MQS estimates can be either positive or negative. The normal test is computationally efficient, but it is important to stress that when the sample size is small it is not appropriate.

We also provide a second, exact option to compute p-values which is valid in the cases of small sample sizes. This second option relies on the fact that the MQS variance component estimate in Eq (4) follows a mixture of chi-square distributions under the null hypothesis. This is because $\mathbf{y}^*$ is assumed to follow a multivariate normal distribution under the modeling assumptions. In particular, $\hat{\sigma}^2 \sim \sum_{i=1}^n \lambda_i\chi_{1,i}^2$, where $\chi_{1,i}^2$ are chi-square random variables with one degree of freedom and $(\lambda_1, \ldots, \lambda_n)$ are the corresponding eigenvalues of the matrix

$$(\hat{\omega}_0^2\mathbf{K}_k^* + \hat{\tau}_0^2\mathbf{M}_k)^{1/2}\mathbf{H}_{k,1}(\hat{\omega}_0^2\mathbf{K}_k^* + \hat{\tau}_0^2\mathbf{M}_k)^{1/2}$$

with $(\hat{\omega}_0^2, \hat{\tau}_0^2)$ being the MQS estimates of (ω^2, τ^2) under the null hypothesis. We can then use the Davies method [64, 81] to compute p-values.

While the Davies method is the appropriate test of choice and is expected to produce calibrated p-values, it can become computationally demanding as the numbers of observed

samples becomes large (see S1 Table). Specifically, the computational complexity of the normal test scales linearly with the number of markers and quadratically with the number of individuals. On the other hand, the computational complexity of the Davies method scales linearly with the number of markers, but cubically with the number of individuals. Therefore, the Davies method can be much slower than the normal test. For example, while analyzing 10,000 markers on a data set with 1,000, 2,500 and 5,000 individuals, the z-test version of MAPIT requires an average of 2.1, 18.9, and 67.6 minutes, respectively. Using the Davies method on these same sets of data, MAPIT requires about 6.1, 108.6, and 654.9 minutes, respectively. Therefore, in practice, we advertise a hybrid p-value computation procedure that uses the normal test by default, and then applies the Davies method when the p-value from the normal test is below the threshold of 0.05. The hybrid procedure combines the advantages of the two different tests and produces calibrated p-values while remaining computationally efficient (again see S1 Table). As we will also show in the results section, the above MQS estimation and testing procedures allow for both accurate and efficient marginal epistatic mapping in moderately sized genetic mapping studies.

Other methods

In this work, we compare MAPIT to two different epistatic mapping approaches. The first is a single-SNP additive association analyses which is fit with a linear regression model by using the -lm argument in the GEMMA software [66–68]. This software is publicly available at http://www.xzlab.org/software.html. The second identifies pairwise interactions directly by implementing an exhaustive search linear model, which we fit by using the --epistasis argument in the PLINK software (version 1.9) [82]. This software is also publicly available at https://www.cog-genomics.org/plink2/epistasis.

Besides estimating and testing marginal epistatic effects for every SNP, we also explore the use of a variance component model to estimate the total contribution of pairwise epistasis onto the phenotypic variance [44, 83, 84]. More specifically, we consider a linear mixed model which partitions the total phenotypic variance using variance components corresponding to additive and pairwise epistatic covariance matrices:

$$\mathbf{y} \quad = \mathbf{g}_1 + \mathbf{g}_2 + \boldsymbol{\varepsilon}, \quad \boldsymbol{\varepsilon} \sim \mathrm{MVN}_n(0, \tau^2 \mathbf{I}_n) \tag{6}$$

where $\mathbf{g}_1 \sim \mathrm{MVN}_n(0, \omega^2 \mathbf{K})$ is the linear effects component; $\mathbf{g}_2 \sim \mathrm{MVN}_n(0, \sigma^2 \mathbf{K}^2)$ is the pairwise interaction component; and ε represents the proportion of phenotypic variance explained by random noise. Here, we let $\{\omega^2, \sigma^2, \tau^2\}$ be corresponding random effect variance terms. The matrix $\mathbf{I}_n$ is an $n \times n$ identity matrix. The covariance matrix $\mathbf{K} = \mathbf{X}\mathbf{X}^{\mathsf{T}}/p$ is the conventional (linear) genetic relatedness matrix, as previous defined. The covariance matrix $\mathbf{K}^2 = \mathbf{K} \circ \mathbf{K}$ represents a pairwise interaction relationship matrix, and is obtained by using the Hadamard product (i.e. the squaring of each element) of the linear kernel matrix with itself [44, 83, 84].

In the presence of population structure and potential stratification effects, we modify Eq (6) by including the top 10 genotype principal components as fixed effects. The modified variance component model can be fitted through the following steps. First, we collect top 10 PCs in a covariate matrix $\mathbf{Z}$. Next, we compute a projection matrix $\mathbf{M} = \mathbf{I} - \mathbf{Z}(\mathbf{Z}^{\mathsf{T}}\mathbf{Z})^{-1}\mathbf{Z}^{\mathsf{T}}$, and multiply it on both sides of the model in Eq (6) to get the following transformed model:

$$\mathbf{y}^* = \mathbf{g}_1^* + \mathbf{g}_2^* + \boldsymbol{\varepsilon}^* \tag{7}$$

where $\mathbf{y}^* = \mathbf{M}\mathbf{y}$; $\mathbf{g}_1^* = \mathbf{M}\mathbf{g}_1$; $\mathbf{K}^* = \mathbf{M}\mathbf{K}\mathbf{M}$; $\mathbf{g}_2^* = \mathbf{M}\mathbf{g}_2$; $\mathbf{K}^{2^*} = \mathbf{M}\mathbf{K}^2\mathbf{M}$; and $\boldsymbol{\varepsilon}_k^* = \mathbf{M}\boldsymbol{\varepsilon}$, respectively.

We apply the first procedure to simulations, and the second procedure to both the simulations and real data analyses. In either case, our goal is to estimate the influence of the total

contribution across pairwise epistatic effects have on the phenotype. We quantify these contributions by examining the proportion of phenotypic variance explained (pPVE) using the following equation defined in [66, 77] for every variance component i:

$$\text{pPVE}_i \propto \frac{\hat{\delta}_i}{n} \text{tr}\left(\sum\nolimits_i\right) \quad \text{and} \quad \sum_i \text{pPVE}_i = 1,$$

where $\Sigma = [\mathbf{K}^*, \mathbf{K}^{2^*}, \mathbf{M}]$. In the current study, with Eq (7), $i = 1, \ldots, 3$. We specifically calculate the pPVEs corresponding to the random effect variance terms $\boldsymbol{\delta} = \{\hat{\omega}^2, \hat{\sigma}^2, \hat{\tau}^2\}$. The variance component that explains the greatest proportion of the overall PVE then represents the most influential effect onto that particular phenotypic response. We implement this model with multiple variance components in the current study by using the −vc argument within the GEMMA software. We also use the standard output (i.e. point estimate and standard error) to conduct an asymptotic normal test to assess the power of this approach.

Software availability

The software implementing MAPIT is freely available at https://github.com/lorinanthony/MAPIT. We use the CompQuadForm R package to compute p-values from the Davies method. The Davies method can sometimes yield a p-value equal exactly to 0 when the true p-value is extremely small [85]. In this case, we report p-values as $P \approx 0$. If this is of concern, one can compute the p-values for MAPIT using Kuonen's saddlepoint method [85, 86] or Satterthwaite's approximation equation [87].

Real data sets

In the present study, we utilize two real data sets: one from the Wellcome Trust Case Control Consortium (WTCCC), and the other from the GEUVADIS Consortium Project. For the first, we specifically used the control samples from the WTCCC 1 study [88] (http://www.wtccc.org.uk/), which consists of 2,938 individuals with 458,868 SNPs following the quality control steps described in detail in a previous study [67].

For the second, we obtained the GEUVADIS data [4] (http://www.geuvadis.org) which contains gene expression measurements for 462 individuals from five different populations: CEPH (CEU), Finns (FIN), British (GBR), Toscani (TSI) and Yoruba (YRI). Following previous studies [89], we focused only on protein coding genes and lincRNAs that are annotated from GENCODE (release 12) [90]. We removed lowly expressed genes that had zero counts in at least half of the individuals, and obtained a final set of 15,607 genes. Afterwards, following previous studies [89], we performed PEER normalization [91] to remove confounding effects and unwanted variations. In order to remove potential population stratification, we quantile normalized the gene expression measurements across individuals in each population to a standard normal distribution, and then quantile normalized the gene expression measurements to a standard normal distribution across individuals from all five populations. In addition to the gene expression data, all individuals in GEUVADIS also have their genotypes sequenced in the 1000 Genomes project [92]. Among the sequenced genotypes, we retained 1,236,922 SNPs that have a minor allele frequency (MAF) above 0.05 and missingness below 0.01. Then, for each gene in turn, we obtained its *cis*-SNPs that are located within either 100 kb upstream of the transcription start site (TSS) or 100 kb downstream of the transcription end site (TES), resulting in a total of 2,735,891 unique SNP-gene combinations with an average of 175 *cis*-SNPs per gene.

In the GEUVADIS data set, we perform four sets of analyses. The first involves using MAPIT with a genetic relatedness matrix $\mathbf{K}_{cis}$, where for the expression of each gene $\mathbf{K}_{cis}$ was

computed using only the corresponding *cis*-SNPs. The second, involves using MAPIT with a genetic relatedness matrix $\mathbf{K}_{trans}$, where for the expression of each gene $\mathbf{K}_{trans}$ is computed using only corresponding *trans*-SNPs located outside of the defined 100 kb *cis*-window. The third analysis corresponds to using MAPIT with a genome-wide genetic relatedness matrix $\mathbf{K}_{GW}$, where $\mathbf{K}_{GW}$ was computed using all SNPs in the study. Besides these analyses, we also performed a fourth analysis to guard against potential residual population stratification. For this analysis, we first compute the top 10 principal components from the genotype matrix, and then collect them in a matrix $\mathbf{Z}$. Next, we regress this matrix of confounding factors onto the expression of each gene, and save the residuals—with which we perform another quantile normalization. We also save the residuals of the genotype matrix after removing the effects of the confounding factors and compute a relatedness matrix $\mathbf{K}_{Pop}$ based on the genotype residuals. Finally, we implement MAPIT on the normalized expression residuals using $\mathbf{K}_{Pop}$.

Results

Simulations: Type I error control

To validate MAPIT and our proposed hybrid testing procedure, in terms of controlling type I error, we carried out a simulation study. Specifically, we utilize the genotypes from chromosome 22 of the control samples in the WTCCC 1 study [88] to generate continuous phenotypes. Exclusively considering this group of individuals and SNPs leaves us with an initial dataset consisting of $n = 2,938$ control samples and $p = 5,747$ markers.

In order to investigate the type I error control, we first subsample from the genotypes for $n = 1,000$, 1,750, and 2,500 subjects. Next, we randomly select 1,000 causal SNPs and simulate continuous phenotypes by using the following two simulation models: (i) a standard model with $\mathbf{y} = \mathbf{X}\boldsymbol{\beta} + \boldsymbol{\varepsilon}$, and (ii) a population stratification model with $\mathbf{y} = \mathbf{Zu} + \mathbf{X}\boldsymbol{\beta} + \boldsymbol{\varepsilon}$, where $\mathbf{X}$ is the genotype matrix, $\mathbf{Z}$ contains covariates representing population structure, and $\mathbf{u}$ are fixed effects. Under the first model, we simulate both the additive effect sizes of each causal SNP and the random noise term from a standard normal distribution, and then we scale the two terms further to ensure a narrow-sense heritability of 60%. In the second model, we introduce population stratification effects into the simulations by allowing the top 5 and 10 genotype principal components (PCs) to make up 10% of the overall phenotypic variance (i.e. through the $\mathbf{Zu}$ term). These population stratification effect sizes are also drawn from a standard normal distribution. Note that, for both settings, the idea of the null model holds because there are no interaction effects, and MAPIT solely searches for significant marginal epistatic effects that are a summation of pairwise interactions. Furthermore, in the cases in which simulations were conducted under model (ii), the genotype PCs were not included while running MAPIT, and no other preprocessing normalization procedures were carried out to account for the added population structure. All evaluations of calibration and type 1 error are strictly based on the linear mixed model presented in Eq (2).

We assess the calibration of MAPIT under both the normal test and the Davies method for each sample size *n*. Fig 1 shows the quantile-quantile (QQ) plots based on simulation model (i), with the application of MAPIT to these null datasets under both hypothesis testing strategies. Similar QQ-plots for data simulated under model (ii) can be found in Supporting Information (see S1 Fig). The normal test heavily relies on the assumption of asymptotic normality—therefore, it is expected to see improvement of performance as the sample size increases. However, as one also expects, the normal test is inaccurate in the extreme tails of the test even for larger sample sizes—hence, the inflation of the normal test p-values in Fig 1. Alternatively, utilizing the Davies method via a mixture of chi-squares allows MAPIT to robustly control for type I error across all sample sizes—even in the presence of population
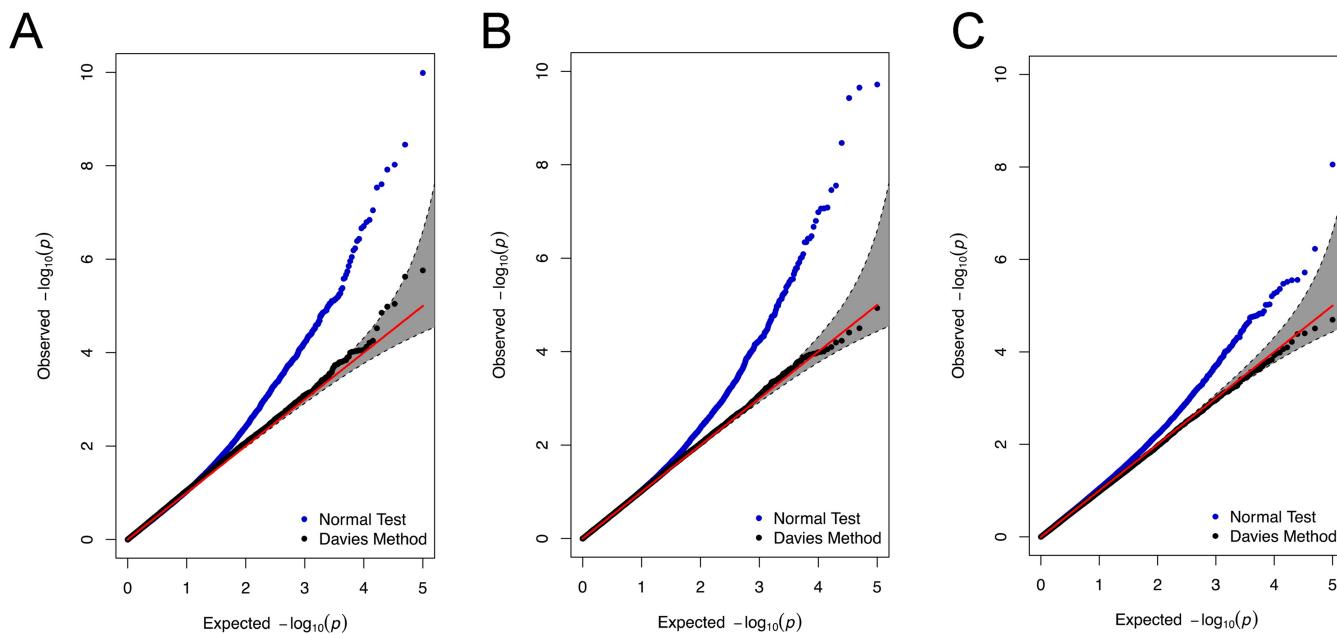
Fig 1. Calibration of p-values produced by MAPIT via QQ-plots. The QQ-plots applying MAPIT to 100 simulated null datasets assuming sample sizes (A) 1,000, (B) 1,750, and (C) 2,500. Blue dots are p-values produced by under the normal test (or z-test), while the black dots represent p-values tested using the Davies method via a mixture of chi-square distributions. The 95% confidence intervals for the null hypothesis of no association are shown in grey.

https://doi.org/10.1371/journal.pgen.1006869.g001

stratification effects. MAPIT's ability to produce calibrated type I error in the presence of population stratification is not surprising, as the model of MAPIT contains a genetic relatedness matrix that has been well known to effectively control for population stratification [66, 70, 76]. Table 1 shows the empirical type I error rates estimated for MAPIT at significance levels $\alpha = 0.05, 0.01$, and 0.001, respectively, for simulations under model (i). Again, similar tables for data simulated under mode (ii) can be found in Supporting Information (see S2 and S3 Tables). As expected based on the QQ-plots under the Davies method, MAPIT controls the type I error rate for reasonably sized datasets, and can be slightly liberal when the sample size is small. Presumably, the liberal behavior of p-values in small samples arises from the fact that frequentist tests do not account for uncertainty in the variance component estimates in the null model. Based on the null simulation results, the Davies method should be the choice of default. However, for computational reasons, we use a hybrid p-value computation procedure (details in Methods and Material) that recalibrates p-value for a SNP using the Davies method

Table 1. Empirical type I error estimates of MAPIT. Each entry represents type I error rate estimates as the proportion of p-values a under the null hypothesis based on 100 simulated continuous phenotypes for the normal test (or z-test) and the Davies method. These results are based on 100 simulated data sets using simulation model (i). Empirical size for the analyses used significance thresholds of $\alpha = 0.05, 0.01$, and 0.001. Sample sizes were set to 1,000, 1,750, and 2,500. Values in the parentheses are the standard deviations of the estimates.

Test	Total Sample Size	$\alpha = 0.05$	$\alpha = 0.01$	$\alpha = 0.001$
Normal Test	$n = 1,000$	0.0598 (0.0061)	0.0180 (0.0031)	0.0047 (0.0013)
	$n = 1,750$	0.0584 (0.0066)	0.0172 (0.0039)	0.0040 (0.0009)
	$n = 2,500$	0.0576 (0.0063)	0.0147 (0.0025)	0.0028 (0.0006)
Davies Method	$n = 1,000$	0.0563 (0.0104)	0.0121 (0.0042)	0.0012 (0.0008)
	$n = 1,750$	0.0528 (0.0083)	0.0108 (0.0023)	0.0011 (0.0004)
	$n = 2,500$	0.0469 (0.0073)	0.0093 (0.0024)	0.0009 (0.0005)

https://doi.org/10.1371/journal.pgen.1006869.t001

when the z-test p-value for the SNP is below the nominal threshold of 0.05. The results we present throughout the rest of the paper will be based on using MAPIT with this hybrid approach.

Simulations: Estimating and identifying marginal epistatic effects

In this section, we use simulation studies to illustrate the advantages of MAPIT in identifying marginal epistatic associations. In addition, besides correctly detecting marginal epistatic associations, we will show that MAPIT can also estimate the marginal epistatic effects reasonably well. Therefore, analogous to SNP heritability estimation settings [67, 69, 75], these variance component estimates can serve as a measurement of the marginal interaction phenotypic variance explained (PVE) by each epistatic causal variant [77].

To test the power of MAPIT, we again consider simulation designs similar to those proposed by previous epistatic analysis studies [63]. First, we assume that the broad-sense heritability is known ($H^2 = 0.6$) [67, 88, 93]. Next, we use the 22nd chromosome of all control cases from the WTCCC 1 study $\mathbf{X}$ (i.e. $n \approx 3,000$ and $p \approx 6,000$) to simulate continuous phenotypes that mirror genetic architectures affected by a combination of additive and pairwise epistatic effects. Specifically, we randomly choose 1,000 causal SNPs to directly affect the phenotype and classify the causal variants into three groups: (1) a small set of interaction SNPs, (2) a larger set of interaction SNPs, and (3) a large set of additive SNPs. In the simulations carried out in this study, SNPs interact between sets, so that SNPs in the first group interact with SNPs in the second group, but do not interact with variants in their own group (the same rule applies to the second group). One may view the SNPs in the first set as the "hubs" in an interaction map. We are reminded that interaction (epistatic) effects are different from additive effects. All causal SNPs in both the first and second groups have additive effects and are involved in pairwise interactions, while causal SNPs in the third set only have additive effects.

The additive effect sizes of all causal SNPs again come from a standard normal distribution or $\boldsymbol{\beta} \sim \text{MVN}(0, \mathbf{I})$. Next, we create a separate matrix $\mathbf{W}$ which holds the pairwise interactions of all the causal SNPs between groups 1 and 2. These SNPs have effect sizes also drawn as $\boldsymbol{\alpha} \sim \text{MVN}(0, \mathbf{I})$. We scale both the additive and pairwise genetic effects so that collectively they explain a fixed proportion of genetic variance. Namely, the additive effects make up ρ%, while the pairwise interactions make up the remaining $(1 - \rho)$%. Once we obtain the final effect sizes for all causal SNPs, we draw errors to achieve the target H^2. The phenotypes are then created by summing all effects using two simulation models: (i) $\mathbf{y} = \mathbf{X}\beta + \mathbf{W}\boldsymbol{\alpha} + \varepsilon$ and (ii) $\mathbf{y} = \mathbf{Z}\mathbf{u} + \mathbf{X}\beta + \mathbf{W}\boldsymbol{\alpha} + \varepsilon$, where $\mathbf{Z}\mathbf{u}$ again represents population stratification. In the latter model, population stratification effects are introduced into the simulations by allowing the top 5 and 10 genotype principal components (PCs) $\mathbf{Z}$ to make up 10% of the overall variation in the trait. The effect sizes for these stratification effects are also drawn as $\mathbf{u} \sim \text{MVN}(0, \mathbf{I})$.

We consider a few scenarios that depend on two parameters:

- $(1 - \rho)$, which measures the portion of H^2 that is contributed by the interaction effects of the first and second groups of causal SNPs. Specifically, the phenotypic variance explained (PVE) by the additive genetic effects is said to be $V(\mathbf{X}\boldsymbol{\beta}) = \rho H^2$, while the PVE of the pairwise epistatic genetic effects is given as $V(\mathbf{W}\boldsymbol{\alpha}) = (1 - \rho)H^2$.

- $p_1/p_2/p_3$, which are the number of causal SNPs in each of the three groups, respectively.

Specifically, we set $\rho = \{0.5, 0.8\}$ and choose $p_1/p_2/p_3 = 10/10/980$ (scenario I), 10/20/970 (scenario II), 10/50/940 (scenario III), and 10/100/890 (scenario IV). Note that scenarios III and IV assume a larger number of interactions than scenario I and II do, and are thus likely to be closer to reality. The particular case where $\rho = 0.5$, the additive and epistatic effects are

assumed to equally contribute to the broad-sense heritability of the simulated phenotypes. The alternative case in which $\rho = 0.8$ is a case where the PVE of the simulated complex traits are dominated by additive effects. We analyze 100 different simulated datasets for each value of ρ, across each of the four scenarios. All of the results described in this section are based on the cases in which phenotypes were simulated under model (i) with $\rho = 0.8$, as this case is a more realistic setting for human traits where epistatic effects only make up a small percentage of the broad-sense heritability. The results for $\rho = 0.5$ can be found in Supporting Information (see S2 Fig). Similar results for all data simulated under model (ii) can also can be found in Supporting Information (see S3 and S4 Figs) Once again, note that in the cases for which simulations were conducted under model (ii), the genotype PCs were not included while running MAPIT, and no other preprocessing normalization procedures were carried out to account for the added population structure. All evaluations of MAPIT are strictly based on the linear mixed model presented in Eq (2).

Fig 2A shows the power results for MAPIT's ability to detect both group 1 and 2 causal variants, respectively, compared across each simulation scenario. Empirical power of MAPIT was estimated as the proportion of p-values below 0.05. We can see MAPIT's ability to detect both groups of causal markers depends on the pairwise interaction PVE explained by each variant. For example in Fig 2A, each causal variant in group 1 is expected to explain $V(\mathbf{W\alpha})/p_1 = 1.2\%$ of the true interaction PVE since in every scenario $p_1 = 10$. In these situations, the cumulative PVE of these markers is great and MAPIT's power is large for all four scenarios (approximately 30% power). Note that this power is similar to MAPIT's ability to detect the group 2 causal markers under Scenario I (i.e. $p_2 = 10$), where each epistatic variant is also expected to explain $V(\mathbf{W\alpha})/p_2 = 1.2\%$ of the interaction PVE. Alternatively, MAPIT exhibits half of the power when detecting the group 2 SNPs in the case of Scenario II (i.e. $p_2 = 20$), as each SNP explains

Fig 2. Empirical power to detect simulated causal interacting makers and estimating their marginal PVE. Groups 1 and 2 causal markers are colored in light red and light blue, respectively. These figures are based on a broad-sense heritability level of $H^2 = 0.6$ and parameter $\rho = 0.8$, estimated with 100 replicates. Here, $\rho = 0.8$ was used to determine the portion of broad-sense heritability contributed by interaction effects. (A) shows the power of MAPIT to identify SNPs in each causal group under significance level $\alpha = 0.05$. The lines represent 95% variability due to resampling error. (B) shows boxplots of the marginal PVE estimates for the group 1 and 2 causal SNPs from MAPIT for the four simulation scenarios. The true PVEs per causal SNP (0.012 for the group 1 SNPs; 0.012, 0.006, 0.0024, and 0.0012 for the Group 2 SNPs) are shown as dashed grey horizontal lines.

https://doi.org/10.1371/journal.pgen.1006869.g002

only $V(\mathbf{W}\boldsymbol{\alpha})/p_2$ = 0.6% of the PVE (approximately 15% power). In addition, MAPIT's power to identify group 1 variants is independent of the number of variants in group 2 (i.e. p_2), suggesting that MAPIT's power depends on the total interaction effects, rather than individual pairwise effects or the number of interacting pairs. The results based on the genome-wide significance threshold are similar and can be found in Supporting Information (see S5 and S6 Figs).

While our main focus is on testing and identifying epistasis, we also assess MAPIT's ability to estimate the contribution of each group 1 and 2 causal SNP to the interaction PVE. Fig 2B show boxplots of these estimates. The true interaction PVE explained by each causal SNP is depicted as the grey dashed lines. These plots show that even though MAPIT's power is directly affected by the epistatic contribution to the phenotypic variation, its ability to correctly estimate the effects of causal interacting SNPs is robust and approximately unbiased. It is important to note that we see MAPIT maintain its estimation ability even when the portion of PVE explained by a set of causal SNPs is very small (i.e. group 2 SNPs in scenario IV). The estimation results are consistent with the well-known robustness of variance component models in estimating PVE in other settings (e.g. estimation of SNP heritability) [67, 69, 75]. Finally, further deviating from our main focus, we also apply a standard variance component model to partition the phenotypic variance into an additive component and an epistatic component following the approach of [44, 83, 84] (details in Methods and Material). Results show that the standard variance component model can also be used to estimate the total contribution of epistasis reasonably well (see S7 Fig), and produces reasonable power at the significance level of 0.05 with a standard asymptotic normal test (see S8 Fig).

Simulations: Power comparisons

Here, we compare the performance of MAPIT with a standard exhaustive search procedure that examines all pairwise interactions to explicitly identify the exact pairs of variants involved in epistatic interactions [55, 56]. Specifically, for the exhaustive search, we consider the PLINK linear model $\mathbf{y} = \mu + \mathbf{x}_i\beta_i + \mathbf{x}_j\beta_j + (\mathbf{x}_i \circ \mathbf{x}_j)\alpha_{ij} + \boldsymbol{\varepsilon}$ and test $H_0: \alpha_{ij} = 0$ for every marker combination of i and j in turn [82]. Keeping notation consistent, $\mathbf{x}_i \circ \mathbf{x}_j$ denotes element-wise multiplication between genotypes i and j, and α_{ij} represents the effect size of their interaction. Note that the exhaustive search procedure is computationally feasible within PLINK because we only have $p \approx 6{,}000$ markers in the simulations.

It is helpful to point out here that the purpose of this comparison is to depict MAPIT as a viable alternative for the exhaustive search procedure. We will show that MAPIT not only can perform a significance test to detect variants involved in epistasis, but also can be used to obtain a prioritized set of variants that are further used to identify pairwise interactions. Our simulation comparisons are thus targeted to illustrate how MAPIT can be used in these two tasks, and how its performance differs from the exhaustive search procedure in different scenarios.

Identifying variants involved in epistasis.   We first compare MAPIT against the PLINK exhaustive search method in identifying variants that are involved in epistasis. For this task, MAPIT can directly perform a significance test and produce a p-value. Here, we note that the power of MAPIT and the exhaustive search method are determined by different factors: the power of the linear interaction method depends on each individual epistatic interaction effect size α_{ij}, while the power of MAPIT, as we have shown in the previous section, depends on the marginal epistatic effects—the summation of interaction effects. Therefore, we would expect MAPIT and the exhaustive search method to be advantageous in different situations (if the exhaustive search method is computationally feasible). In particular, we would expect the exhaustive search method to be more powerful in scenario I (and II) where each individual

interaction effect is large, and MAPIT to be more powerful in scenario (III and) IV where each individual interaction effect is small but the marginal epistatic effect remains large. Furthermore, MAPIT can naturally account for population stratification via the included genetic relatedness matrix, while the exhaustive search method requires including genotype PCs as covariates to control for such confounding effects. Therefore, we would also expect MAPIT to be robustly more powerful when there are confounding population stratification effects that are not explicitly taken into account. To validate our expectations, we again generate continuous outcomes using the same two previously described simulation schemes: (i) $\mathbf{y} = \mathbf{X}\beta + \mathbf{W}\alpha + \varepsilon$ and (ii) $\mathbf{y} = \mathbf{Z}\mathbf{u} + \mathbf{X}\beta + \mathbf{W}\alpha + \varepsilon$. Once again, all results described in the main text are based on model (i) with $\rho = 0.8$, while all other results can be found in Supporting Information (see S9–S13 Figs).

We evaluate MAPIT's and PLINK's ability to accurately identify marginal epistatic effects for markers in each of the two causal groups. The criteria we use compares the false positive rate (FPR) with the rate at which true variants are identified for each model (TPR). Fig 3 depicts the ability of MAPIT and PLINK to detect causal variants in groups 1 and 2. In particular, these plots depict the portion of causal markers discovered after prioritizing all of those considered in order of their significance. We assess the marginal epistatic detection in the PLINK exhaustive search by first running the previously described pairwise linear model, ordering the resulting p-values for each possible interaction, and drawing a power curve for identifying the SNPs that are members of simulated causal groups 1 and 2. For example, if the top p-values from the exhaustive search are interactions SNP1-SNP2, SNP2-SNP3, SNP4-SNP5, and only SNP2 is the true causal epistatic variant, then the top three pairs only marginally identify 1 true variant and 4 false variants.

As expected, while the power of MAPIT depends on the pairwise interaction PVE explained by each SNP, the power of the exhaustive search depends on the individual interaction effect size. For example, the power of the exhaustive search to detect group 1 causal epistatic SNPs is dependent on the number of group 2 causal SNPs, which also determines the interaction effect size in simulations. Therefore, while the exhaustive search exhibits higher power in the sparse scenario where there are only a small number of interactions each with a large effect size (e.g. scenarios I and II), its power quickly decays in the more polygenic scenario where there is a large number of interactions, each with a small effect size (e.g. scenarios III and IV). MAPIT is able to perform well in the more realistic polygenic scenarios (III and IV) by modeling the marginal epistatic effects of each variant, allowing the detection of epistatic variants not to be dependent on the individual pairwise interaction effect size. Importantly, MAPIT remains powerful even in the presence of population stratification, as it can effectively control for population stratification with the included genetic relatedness matrix. In contrast, the exhaustive search approach in PLINK does not explicitly control for population stratification, and can suffer from power loss in the presence of stratification especially when the total epistatic contribution (i.e. $1 - \rho$) is small (see again S11 and S13 Figs).

We are reminded that another advantage to MAPIT is the reduced space it must search over, as MAPIT only requires p tests for a data set with p genetic markers. Therefore, MAPIT is expected to exhibit a computational advantage over this type of exhaustive search approach in moderate size genetic mapping studies with millions of markers.

Identifying pairwise interactions. Although we have focused on identifying marginal epistatic effects so far, MAPIT can also be used to facilitate the identification of pairwise (or high-order) epistatic interactions. In addition to comparing MAPIT with the exhaustive search method from PLINK, we also consider another common approach for identifying epistatic pairs—a two-step filtering association mapping procedure [51, 55, 58]. These types of filtering methods often first apply a marginal (additive) single-SNP test to identify associated genetic
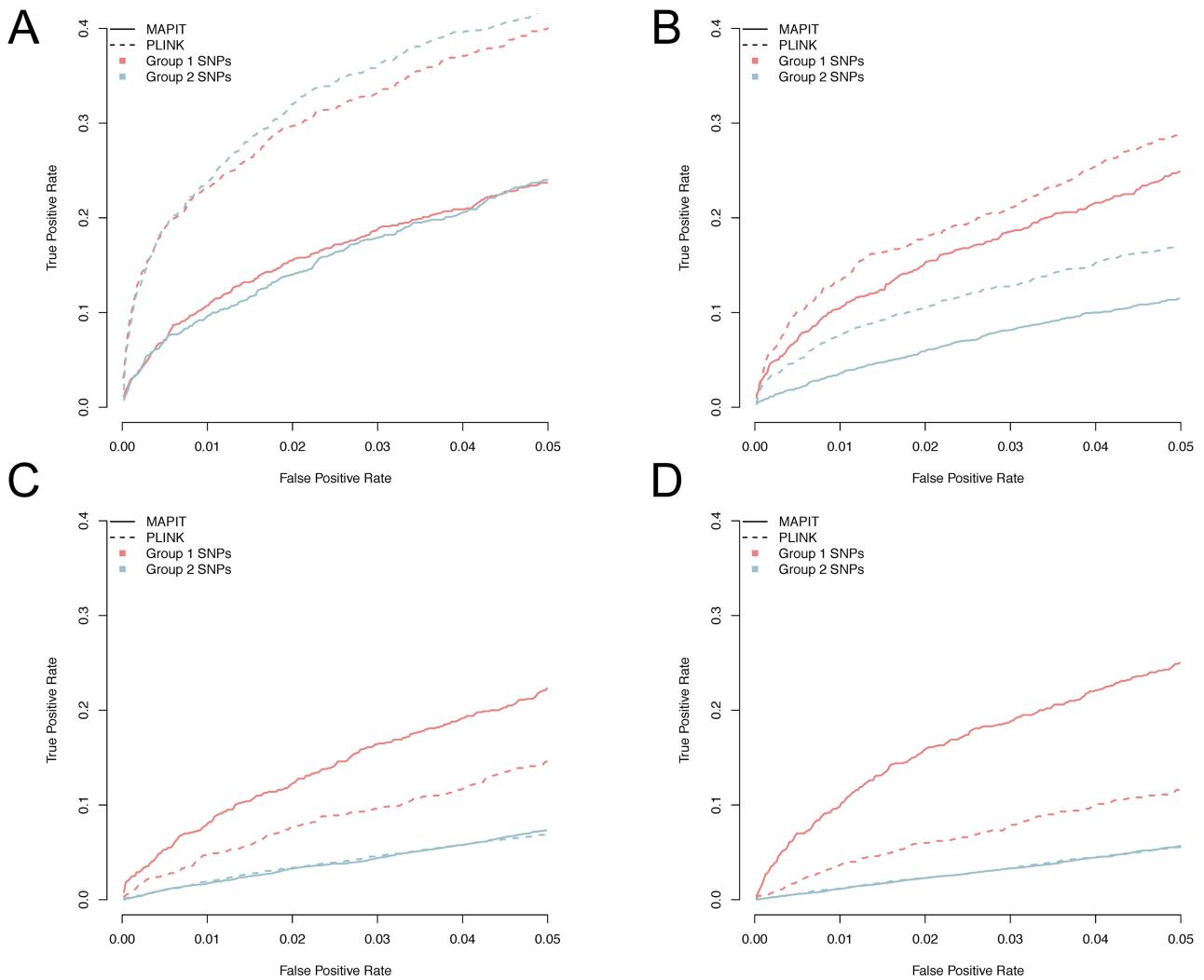
Fig 3. Power analysis for detecting group 1 and group 2 causal SNPs. We compare the mapping abilities of MAPIT (solid line) to the exhaustive search procedure in PLINK (dotted line) in scenarios I (A), II (B), III (C), and IV (D), under broad-sense heritability level $H^2 = 0.6$ and $\rho = 0.8$. Here, $\rho = 0.8$ was used to determine the portion of broad-sense heritability contributed by interaction effects. Group 1 (light red) and group 2 (light blue) causal SNPs. The x-axis shows the false positive rate, while the y-axis gives the rate at which true causal variants were identified. Results are based on 100 replicates in each case.

variants with non-zero additive effects, and then focus on the identified variants to test all pairwise interactions between them. Depending on the correlation between the marginal additive effect size and the probability of being involved in epistasis with SNPs genome-wide, these filtering methods can be more powerful than the exhaustive search strategy mentioned in the previous section—not to mention they are certainly much more computationally efficient. However, for any trait, because there is no expectation that SNPs involved in epistasis will always have large additive effects, these filtering methods will not always outperform the exhaustive search method, and can sometimes be significantly under powered (as our simulations and real data application will show). Here, instead of using the additive test, we propose using MAPIT as the initial filter. We hypothesize that the initial list of associated SNPs from MAPIT will be more robust and more likely capture epistatic effects, as MAPIT directly prioritizes SNPs based on marginal epistatic effects. By using marginal epistatic evidence in the

initial filtering step, we expect MAPIT to outperform the previous common procedure of using a linear model for filtering.

In this set of simulations, we utilize the same subset of real genotypes used for the marginal epistatic simulations in the last section [88], and again generate phenotypes under the same four simulation scenarios with the same two simulation models where pairwise interactions are well defined. After randomly selecting the three sets of causal SNPs and creating their pairwise interactions, we run MAPIT and a single-SNP additive linear model (via GEMMA) [66] using all variants. We also reuse the PLINK exhaustive search, again as a baseline comparison. For MAPIT and the single-SNP linear model in GEMMA, we rank each variant according to their marginal p-values. The top 100 SNPs identified by both models are then selected, and all pairwise interactions among them are tested using a linear model that controls for the two main effects. For the PLINK exhaustive search, we simply rank the top 100^2 interactions to assess pairwise power.

Fig 4 compares the power of the filtering procedures using the two different methods as an initial step. Phenotypes used to create this figure were generated under each scenario with broad-sense heritability $H^2 = 0.6$. As in previous sections, all results described in this section are based on model (i) with $\rho = 0.8$, and all other results can be found in Supporting Information (see S14 and S15 Figs). Compared with the single-SNP test, filtering SNPs using MAPIT provides more power in finding true pairwise epistatic interactions. In fact, even for the cases in which the marginal additive effects contribute to a majority of the broad-sense heritability (i.e. $\rho = 0.8$), using MAPIT as the initial filtration procedure (as opposed to the single-SNP additive linear model) provides more power for finding exact causal epistatic pairs. This improvement comes from the fact that MAPIT allows the ranking of variants to be based on their marginal epistatic effects, rather than their marginal additive effects. Therefore, the set of SNPs identified by MAPIT in the first step already contains variants that capture epistatic effects, thus resulting in higher power in the second step to identify epistatic interaction pairs. In addition, similar to the simulation comparison in the previous subsection, MAPIT and the exhaustive search procedure are advantageous in different settings: the exhaustive search procedure is again more powerful in the sparse setting where each individual pairwise interaction is large (i.e. scenarios I and II) while MAPIT gains an advantage in the polygenic setting where there a large number of interactions each with small effects (i.e. scenarios III and IV). Again, in the presence of population stratification, MAPIT remains powerful while the exhaustive search procedure suffers from substantial power loss (see again S15 Fig). Overall, MAPIT also represents an attractive alternative to identifying pairwise interactions.

Detecting epistasis in GEUVADIS

We assess MAPIT's ability to detect epistasis in a quantitative trait loci (QTL) association mapping study for gene expression levels (i.e. eQTL study). Often times, eQTL studies deal with SNP effect sizes (on gene expression levels) that are orders of magnitude larger than that (on organism-level traits) from GWASs [2–5], thus facilitating in the identification of epistasis. Indeed, recent studies have started to reveal an initial set of epistatic interactions that underlie gene expression variation [37, 94, 95]. By applying MAPIT to eQTL studies, we hope to better understand the genetic architecture that underlie gene expression variation.

The specific data set that we consider in this section features 462 individuals from five different populations whose gene expression data was collected by the GEUVADIS consortium [4]. These individuals also have their genotypes sequenced by the 1000 Genomes project [92]. In order to identify potential QTLs involved in associated pairwise epistatic interactions, we exclusively use MAPIT to analyze variants that passed quality control filters and were located
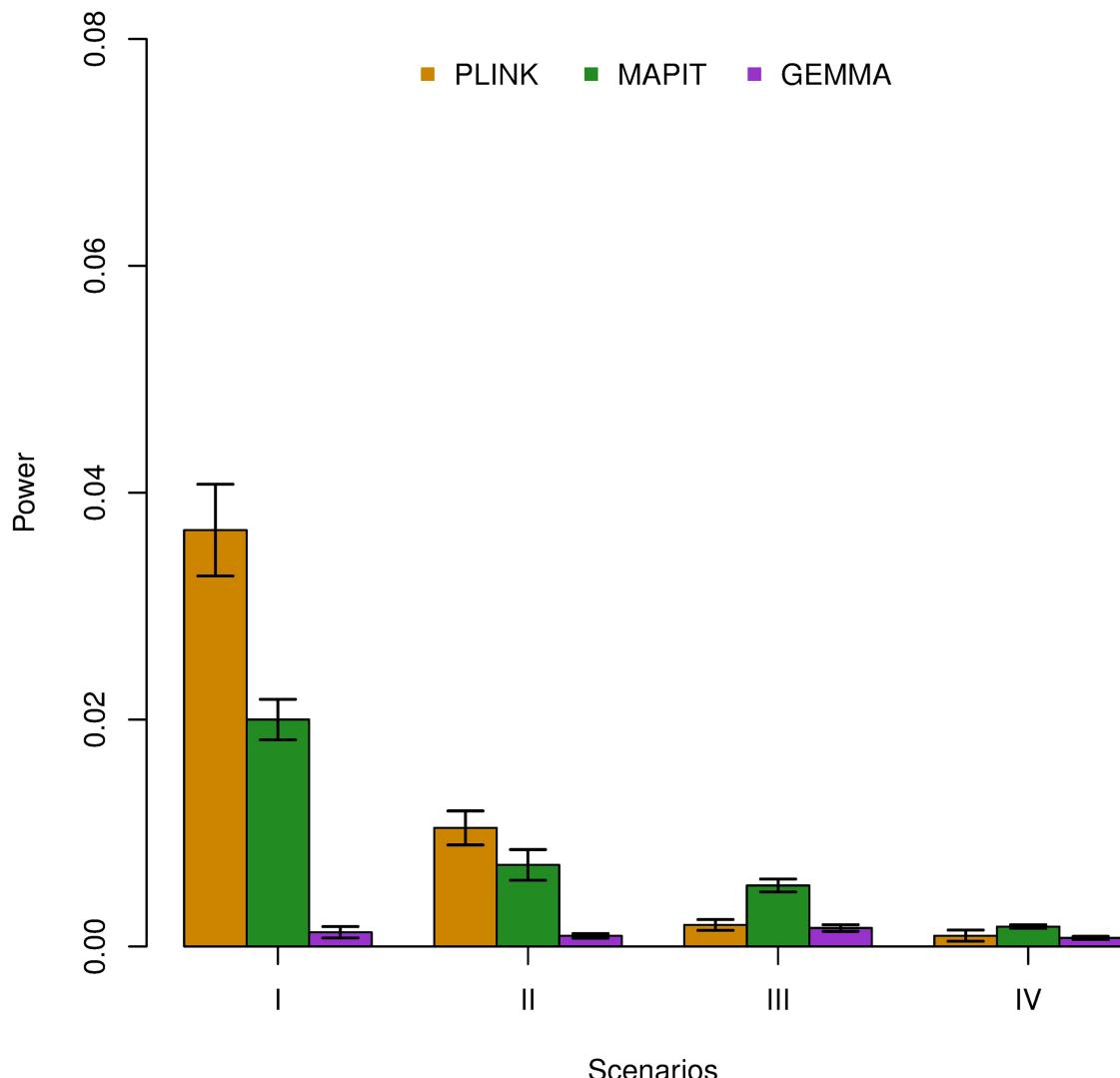
Fig 4. Empirical power of exhaustive search procedures to detect epistatic pairs. Here, the effectiveness of MAPIT (green) as an initial step in a pairwise detection filtration process is compared against the more conventional single-SNP testing procedure, which is carried out via GEMMA (purple). In both cases, the search for epistatic pairs occurs between the top 100 significant marginally associated SNPs are considered. We use the fully exhaustive search model in PLINK (orange) as a baseline comparison. We compare the three methods in all scenarios (x-axis), under broad-sense heritability level $H^2 = 0.6$. Here, $\rho = 0.8$ was used to determine the portion of broad-sense heritability contributed by interaction effects. The y-axis gives the rate at which true causal epistatic pairs were identified. Results are based on 100 replicates in each case. The lines represent 95% variability due to resampling error.

within 100 kb of each gene of interest (Materials and methods). Such variants represent likely *cis*-acting QTL, which are more readily identifiable in small sample sizes than trans-QTL [2–5]. Overall, we apply MAPIT to a final data set that consists of approximately 16,000 genes, 1.2 million SNPs, and 2.7 million SNP-gene combinations.

To remove population stratification and other confounding effects, we have removed top factors from the gene expression matrix and normalized the gene expression data within each of the five populations separately—all before performing a final joint normalization [4] (details in Methods and Material). The results of MAPIT presented in this section are based on using additive and epistatic relatedness matrices derived from a covariance matrix $\mathbf{K}_{cis}$, where for the

expression of each gene K_{cis} was computed using only the corresponding *cis*-SNPs. While using K_{cis}, MAPIT tests the summed epistatic effects between a given *cis*-SNP and all other *cis*-SNPs within the same gene. The primary reason that we present the main results based on K_{cis} is to allow for a fair comparison with the exhaustive search method (details below)—which, due to computational reasons, can only be applied to examine all *cis*-pairs. To assess whether or not these initial results are sensitive to the choice of covariance matrix, we also implement MAPIT using a genetic relatedness matrix K_{trans}, where for the expression of each gene K_{trans} was computed using only the corresponding *trans*-SNPs located outside the *cis*-window (Methods and Material). Using MAPIT with K_{trans} assesses the summed epistatic effects between a given *cis*-SNP and all other *trans*-SNPs. Lastly, we consider the implementation of MAPIT with a genome-wide genetic relatedness matrix K_{GW}, where K_{GW} was computed using all SNPs in the study (Methods and Material). Here, using MAPIT with K_{GW} tests the summed epistatic effects between a given *cis*-SNP and all SNPs genome-wide. Intuitively, using K_{cis} will be more powerful than using either K_{trans} or K_{GW} if epistatic interactions are more likely to happen between *cis*-SNP pairs, rather than between *cis*-SNP and genome-wide SNP pairs—however, less powerful otherwise. In addition to these three sets of analyses, to guard against any potential residual population stratification, we also removed the effects of the top 10 genotype principal components and used the residual expression data together with a K_{Pop} computed using the genome-wide residual genotype data for a further analysis. The purpose of the additional analyses is to highlight the robustness of the results found using MAPIT.

To contrast MAPIT's marginal association findings, we also directly compare results from the single-SNP additive model via GEMMA and the fully exhaustive search model in PLINK. From this point forward, we will refer to QTL identified by MAPIT as marginally epistatic QTL (*mepiQTL*), the QTL detected by GEMMA as the more conventional expression QTL (*eQTL*), and the QTL found by PLINK as epistatic QTL (*epiQTL*). Similarly, we will refer to genes that have at least one mepiQTL as *mepiGenes*, genes that have at least one eQTL as *eGenes*, and genes that have at least one epiQTL as *epiGenes*.

In this analysis, a significant marginal association for a particular SNP identified by MAPIT or GEMMA was determined by using a gene specific Bonferroni-corrected significance p-value threshold $P = 0.05/\sum s_i = 1.828 \times 10^{-8}$, where s_i is the number of *cis*-SNPs for gene i. For PLINK, a single SNP was deemed marginally significant if it belonged to a epistatic pair with a p-value below the genome-wide threshold $P = 1.09 \times 10^{-10}$ (i.e. Bonferroni correction for a total of 455,801,241 examined cis-SNP pairs). While using the genetic relatedness matrix K_{cis}, MAPIT identified a total of 3,434 mepiQTL across 228 different mepiGenes that satisfied this marginal significance rule. Additionally, while using the covariance matrix K_{trans}, MAPIT detected a total of 2,160 across 130 mepiGenes. Similarly, MAPIT also identified a total of 2,160 mepiQTL across 130 mepiGenes when using K_{GW} (i.e. identical to that identified by K_{trans}), and this number changed to 3,056 mepiQTL across 184 different mepiGenes after correcting for residual population stratification and using K_{Pop}. GEMMA, on the other hand, found 55,645 significant eQTL across 1,417 different eGenes, and no significant eQTL or eGenes after correction for potential residual population stratification. Note that the former number of eGenes as detected by GEMMA is similar to that from the original research [4], with slight differences most likely due to data set variations (e.g. data origins, preprocessing measures, etc.). Lastly, PLINK identified 14,722 significant epiQTL spanning across 99 epiGenes prior to accounting for any residual confounding effects, and 17,286 significant epiQTL spanning across 102 epiGenes after the extra correction. The amount of overlap between the mepiQTL/mepiGenes detected by MAPIT, the eQTL/eGenes identified by GEMMA, and the epiQTL/epiGenes found by PLINK is explicitly specified in Supporting Information (see S4 and S5 Tables).
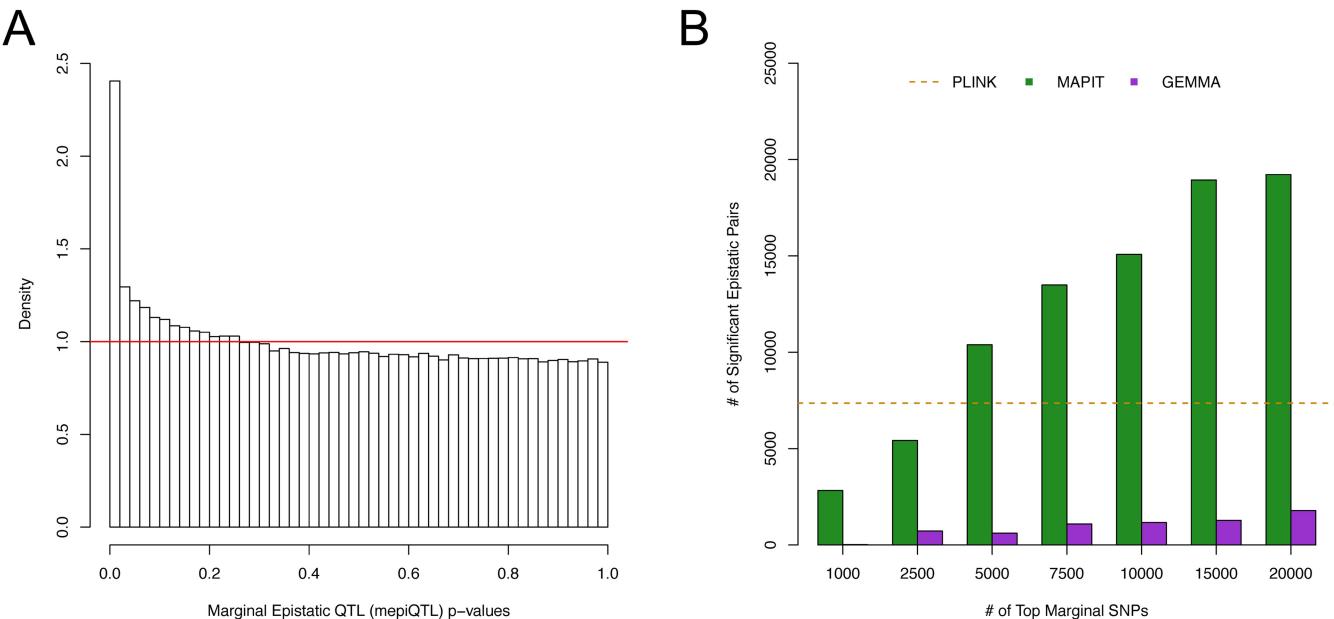
Fig 5. Comparison of epistatic filtration methods with MAPIT and GEMMA on the GEUVADIS data set. All of these results are based on using MAPIT with genetic relatedness matrix $\mathbf{K}_{cis}$. (A) shows a histogram of the MAPIT p-values for all variants in the GEUVADIS data set. The horizontal red line corresponds to a uniform distribution of p-values. (B) shows the number of significant pairwise interactions (y-axis) identified by MAPIT (green) and GEMMA (purple) when searching between the top {1000, 2500, 5000, 7500, 10000, 15000, 20000} marginally associated variants (x-axis). We use the number of significant pairs identified by fully exhaustive search model in PLINK as a baseline comparison (orange dotted line). This image shows the distributions of genome-wide significant epistatic pairs as found by each method. An interaction for MAPIT and GEMMA was deemed signifiant if it had a joint p-value below the threshold $P = 0.05/(\sum_i q_i(q_i - 1)/2)$, where q_i is the number of top variants located in the *cis*-window of gene i. In the case of PLINK, we consider two variants to be a significantly associated epistatic pair if they have a joint p-value below the threshold $P = 1.09 \times 10^{-10}$, which corresponds to the Bonferroni-correction that would be used if we examined all possible genome-wide SNP pairs across all genes in the final data set. Overall, PLINK detected 7,361 significant epistatic pairs.

https://doi.org/10.1371/journal.pgen.1006869.g005

The histogram of the MAPIT p-values for all SNP-gene combinations, while using $\mathbf{K}_{cis}$, is presented in Fig 5A with a corresponding QQ-plot of the $-\log_{10}$ p-values presented in Supporting Information (see S16A Fig). Both of these figures illustrate strong signals on a background of uniformly distributed p-values. Similar results for MAPIT with $\mathbf{K}_{trans}$, $\mathbf{K}_{GW}$, and $\mathbf{K}_{Pop}$ can be found in Supporting Information (see S16B, S16C, S16D, S17A, S17B, and S17C Figs). S6–S9 Tables also list the p-values for all significant mepiQTL as computed via a MAPIT scan over the *cis*-windows of each gene, with and without correction for population stratification. The distribution of locations for mepiQTL and eQTL, relative to the gene transcription start site (TSS) and the gene transcription end site (TES), is depicted in Fig 6 (see also S18 Fig). Consistent with evaluations of other QTL association mapping studies [2–5], eQTLs detected by GEMMA are mostly enriched near TSS. In contrast, mepiQTLs are enriched near the TES in addition to the TSS, with distance to genes showing a slightly wider spread pattern than eQTLs.

Since MAPIT produces a single p-value for each tested variant, we may visualize the specific genomic locations that exhibit epistasis. Fig 7 displays zoomed-in manhattan plots for three of the twenty-two chromosomes where some of the most notable significant marginal epistatic effects were detected under the marginal genome-wide significance threshold ($P = 1.828 \times 10^{-8}$). Figures depicting the genome-wide epistatic scans of the other chromosomes can be found in Supporting Information (see S19–S24 Figs). Note that since there could be multiple p-values for a single SNP (i.e. its association evidence for multiple genes), we choose to display the minimum p-value as the summary statistic for any given SNP. We stress

that the interpretation of these images is slightly different than what is used for traditional manhattan plots. Specifically, in these figures, spikes across chromosomes suggest loci where members involved in epistatic interactions can be found.

In order to search for exact epistatic pairs among cis-SNPs through the filtering approaches, we took all significant mepiQTL and eQTL, and analyzed the pairwise interactions between them. This comparison allows us to assess the power of MAPIT and GEMMA as filtering approaches within the context of real data. Similar to what was done in the simulation studies, both filtering procedures were carried out by first ranking SNPs by either their mepiQTL or eQTL p-values, and then searching for associated epistatic pairs between the top v SNPs. Interactions between two mepiQTL or eQTL were then called significant if they had a joint p-value below a gene specific Bonferroni corrected threshold. Briefly, this threshold is computed as $P = 0.05/(\sum_i q_i(q_i - 1)/2)$, where q_i is the number of top variants (among the top v SNPs) located in the *cis*-window of gene i. Once again, we applied the fully exhaustive search model in PLINK as a baseline power comparison, in which we examined all of the *cis*-SNP pairs for each gene. Note that for PLINK we only consider cis-SNP combinations as it was not computationally feasible to perform an absolute complete exhaustive search (i.e. every gene pair between all 1.2 million SNPs for each of the 16,000 genes). Fig 5B (and S17D, S17E, and S17F Fig) depicts the number of significant pairwise interactions identified by MAPIT (with different **K** matrices) and GEMMA when searching between the top $v = \{1000, 2500, 5000, 7500, 10000, 15000, 20000\}$ marginally associated variants. Altogether, the exhaustive search method in PLINK identified 7,361 significant epistatic pairs before the correction of residual confounding effects, and 8,643 significant pairwise interactions after the correction. These benchmarks are represented by the dotted lines in Fig 5B, S17D, S17E, and S17F Fig, respectively.

As demonstrated in the numerical experiments, using MAPIT as the initial filtration procedure (as opposed to the single-SNP additive model) efficiently provides more power to finding significant epistatic pairs. Moreover, considering interactions amongst just the top 2,500 mepiQTL (in any of the considered settings for MAPIT) almost results in the same total number of significant epistatic pairs that is to be discovered by the fully exhaustive search model from PLINK. As previously shown, these results may be due to MAPIT's ability to marginally detect the "hub" SNPs of interactions. For example, under the expression for gene *C16orf88*, the SNP rs11645910 (MAPIT $P \approx 0$) is a member of many of the top significant epistatic pairs. We also note that 36 of the 228 epistatic associated genes identified by MAPIT with $\mathbf{K}_{cis}$ have been verified in previous analyses on a different RNAseq data set from the TwinsUK cohort [37]. Similarly, 26 of the 120 mepiGenes discovered by MAPIT with $\mathbf{K}_{trans}$ and $\mathbf{K}_{GW}$, and 35 of the 184 mepiGenes discovered by MAPIT with $\mathbf{K}_{Pop}$ after correction for residual confounders, have been verified in the same study.

In order to better explain why MAPIT was able to identify significant epistatic pairs in this study, we refer back to the variance component modeling approach [44, 83, 84] we used in simulations to evaluate the overall contribution of pairwise epistasis to the PVE for the expression of each gene (details in Methods and Material). Again, the basic idea behind dissecting the makeup of the PVE is using a linear mixed model with multiple variance components to partition the phenotypic variance into two distinct components: a linear component and a pairwise interaction component. Disregarding any random noise, we quantify the contribution of the two components by examining the proportion of PVE (pPVE) explained by that component. In Supporting information, we illustrate the estimates of the pPVE decomposition by additive effects and pairwise epistasis for all genes (see S25 Fig). In this particular data set, we find that the mean pPVE for the pairwise interaction component is approximately 10%, which is consistent with previous studies on the same data [96]; while the additive effects only explain about 3.5% on average. To put this into better context, for the gene *C16orf88*, pairwise
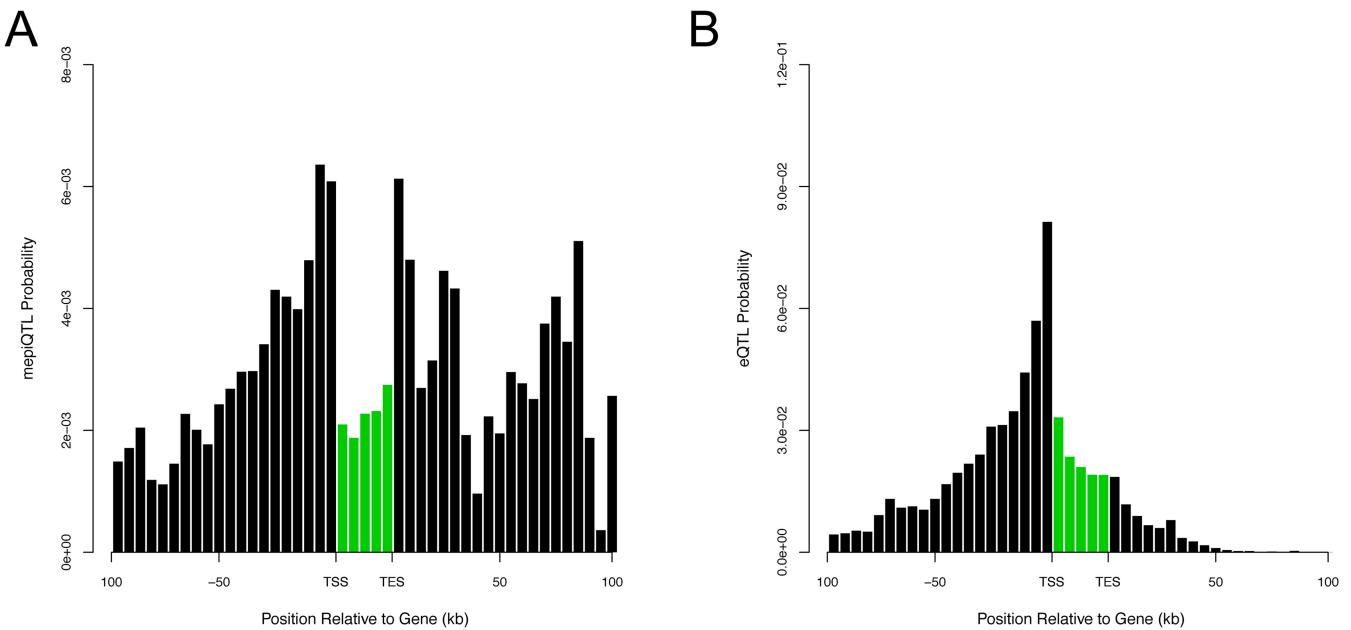
Fig 6. Enrichment of eQTL and mepiQTL SNPs in GEUVADIS data set. Shown here are the distribution of locations for significant SNPs, relative to the 5′ most gene transcription start site (TSS) and the 3′ most gene transcription end site (TES). (A) displays the marginally epistatic QTL (mepiQTL) detected by MAPIT using genetic relatedness matrix $\mathbf{K}_{cis}$. (B) corresponds to the expression QTL (eQTL) identified by the single-SNP via GEMMA. The x-axis of each plot divides a typical *cis*-candidate region into a series of bins. The y-axis plots the number of SNPs in each bin that have a p-value less than a gene specific Bonferroni-corrected significance p-value threshold $P = 0.05/\sum_i s_i$, where s_i is the number of *cis*-SNPs for gene *i*, divided by the total number of SNPs in that bin. Bars in green denote the region bounded by the TSS and TES, with gene lengths divided into 20 bins for visibility—because the gene body is thus artificially enlarged, SNP density within genes cannot be directly compared with SNP density outside of genes.

https://doi.org/10.1371/journal.pgen.1006869.g006

epistatic effects are estimated to explain approximately 5% of the PVE, while additive effects are estimated to only account for 3×10^{-3}%. In fact, the pairwise order component actually explains a larger proportion of phenotypic variance than the linear component in the expression of 7,704 out of 15,607 genes.

Finally, we also want to point out one important caveat for mapping epistasis in real data: in the analyses of genetic mapping studies, apparent epistasis inferred by any epistatic mapping methods can sometimes be explained by same-locus additive effects [41]. This means that the results from all methods (MAPIT or the exhaustive search procedure or the additive-effect based filtering procedure) could be confounded by additive effects of untyped SNPs or uncontrolled SNPs in the same region, even though the power comparison among these methods remains fair. Dealing with these contingencies is difficult because it is impossible to precisely control for the additive fixed effects of all SNPs that reside in the same locus. Therefore, we caution against the over-interpretation of our analysis results in GEUVADIS and simply use the GEUVADIS data as an illustration on how MAPIT can be used as a first step towards understanding the genetic architecture of phenotypic variation.

Discussion

We have presented MAPIT, a novel method and strategy for detecting variants that are involved in epistasis in genetic mapping studies. For each variant in turn, MAPIT estimates and tests its marginal epistatic effect—the combined epistatic effect between the examined variant and all other variants. By modeling and inferring the marginal epistatic effects, MAPIT can identify variants that exhibit non-zero epistatic interactions with any other variant without

Fig 7. Select chromosome-wide scans for epistatic effects in GEUVADIS data set. Depicted are the $-\log_{10}(P)$ transformed MAPIT p-values of quality-control-positive *cis*-SNPs plotted against their genomic position in chromosomes (A) 1, (B) 6, and (C) 22, respectively. Note that MAPIT was implemented with $\mathbf{K}_{cis}$. Here, the epistatic associated genes are labeled (blue). The (red) horizontal line indicates a genome-wide significance threshold ($P = 1.828 \times 10^{-8}$). Note that all panels are truncated at $-\log_{10}(P) = 10$ for consistency and presentation, although for some genes there are strongly marginally epistatic associated markers with p-values $P \approx 0$.

https://doi.org/10.1371/journal.pgen.1006869.g007

the need to identify the specific marker combinations that drive the epistatic association. Therefore, MAPIT represents an attractive alternative to standard methods [54–56, 63] for mapping epistasis. With both simulations and real data applications, we have illustrated the benefits of MAPIT.

In the present study, we have focused on estimating and testing marginal epistatic effects in the presence of pairwise interactions with MAPIT. MAPIT can also be easily extended to

detect variants that are involved in higher-order interactions. Specifically, in the presence of higher-order interactions, we can introduce extra random effects terms to represent the combined higher-order interaction effects between the examined variant and all other variants—this would simply mean adding an extra random effects term for each extra higher-order of interactions. Under the normality assumption of the interaction effect sizes, the introduced random effects terms would all follow multivariate normal distributions, with the covariance matrices determined as a function of the Hadamard product of the additive genetic relatedness matrix [44, 84, 97]. Therefore, we can use a multiple variance component model with additional variance components to map epistatic variants in the presence of higher-order interactions. From there, we can test the variance components jointly to identify variants that are involved in any order of epistatic interactions. We can test each variance component separately to identify variants that are involved in a particular order epistatic interaction. Or, better still, we can perform variable selection on the variance components to identify which higher order interaction a particular variant of interest is involved in. Extending MAPIT to mapping high-order interactions will likely provide further insights into the epistatic genetic architecture of various traits and diseases.

We have focused on mapping epistasis for quantitative traits. For case-control studies, one may be tempted to follow previous approximate approaches of treating binary phenotypes as continuous traits and apply MAPIT directly [67, 98]. However, it would be desirable to extend MAPIT to accommodate case-control data or other discrete data types in a principled way. Two variance component models are available for handling case-control data, and each has its advantages and drawbacks. The first model is the liability threshold model, which models the liability score underlying the binary trait with a variance component model [79, 98]. The liability threshold model has been widely used for estimating heritability of common diseases, but relies on an asymptotically normal test, which, as is evident with our simulations, may fail to properly control for type I error at the genome-wide significance level for association tests. The second model is the logistic mixed model that has been well established in the statistics literature [99–102], and has been recently applied to perform association tests in case-control studies [103] as well as in RNA sequencing and bisulfite sequencing studies [104, 105]. However, unlike the liability threshold model, it is not straightforward to define and partition the phenotypic variance into various genetic components under the logistic mixed model. Therefore, future studies are needed to extend MAPIT to case-control studies by either unifying the two models or developing new methods that can perform rigorous hypothesis tests while enabling genetic partitioning of phenotypic variance.

In its current form, we have focused on demonstrating MAPIT with a variance component model. The variance component model in MAPIT effectively assumes that the interaction effect between the examined variant and every other variant follows a normal distribution. This normality assumption and the resulting variance component model have been widely used in many areas of genetics. For example, variance component models are used in rare variant tests to combine the additive effects of multiple rare variants to improve association mapping power [64, 65]. Similarly, variance component models are used to jointly model all genome-wide SNPs at once for estimating SNP heritability [67, 69]. Studies have already shown that variance component models produce unbiased estimates regardless of whether or not the underlying effect sizes follow a normal distribution, and are reasonably robust even when the model is severely misspecified [67, 69]. However, like any statistical model, the inference results of variance component models can be affected when the modeling assumptions are not fully satisfied. For example, recent studies have shown that the linkage disequilibrium (LD) pattern of causal SNPs can cause estimation bias that is either minor allele frequency (MAF) mediated or non-MAF-mediated [50, 75]. Such LD-biases likely affect MAPIT in a

similar fashion. Therefore, adapting the approaches taken in [50, 75] or developing a more realistic modeling assumption will likely improve the robustness of MAPIT even further. Fortunately, MAPIT can easily be extended to incorporate other effect size assumptions. Indeed, the main idea in MAPIT of mapping marginal epistatic effects is not restricted to the particular variance component model we examine here, nor is it restricted to the normality assumption of the interaction effect sizes. Therefore, we can incorporate sparsity-inducing priors for effect sizes if the number of interaction pairs is known to be small *a priori*. Alternatively, we can use the recently developed hybrid effect size prior that has been shown to work well under a variety of effect size distributions [67]. Different interaction effect size assumptions can be advantageous under different genetic architectures and incorporating them in different scenarios will likely improve the power of MAPIT further.

We have only compared MAPIT with two commonly used epistatic mapping methods that include an exhaustive search method and an additive effect prioritization method. There are many other novel methods that have been developed recently [53, 57, 60–62]. For example, a recently proposed partition retention method partitions individuals into different genotype groups that are defined based on the pairwise or high-order combinations of their genotypes (e.g. a total of 81 genotype groups for four SNPs that each have three genotype classes) [106]. More specifically, this method first computes the phenotypic variance across these genotype groups, and then examines each SNP in the combination by testing whether the SNP adds a significant contribution to the phenotypic variance across the groups. Despite its computational intensity, the partition retention method produces promising results. It would thus be important to compare MAPIT with the partition retention method, as well as others, in the future.

There are many other potential extensions of MAPIT. We have only focused on analyzing one phenotype at a time in this study. However, it has been extensively shown that modeling multiple phenotypes can often dramatically increase power [68, 74]. Therefore, it would be interesting to extend MAPIT to take advantage of phenotype correlations to identify pleiotropic epistatic effects. Modeling epistasis in the context of multiple phenotypes could be highly non-trivial, as we need to properly model the shared epistatic components between phenotypes, in addition to the shared additive effects between phenotypes. Modeling strategies based on the multivariate linear mixed model (mvLMM) [68, 74] could be helpful here.

MAPIT is not without its limitations. Perhaps the most noticeable limitation is that MAPIT cannot be used to directly identify the interaction pairs that drive individual variant association. In particular, after identifying a variant involved in epistasis, it is still unclear which variants it interacts with. Thus, despite being able to identify SNPs that are involved in epistasis, MAPIT is unable to directly identify detailed interaction pairs. However, we argue that being able to identify variants that are involved in epistasis is often an important first step towards identifying and understanding detailed epistatic associations. In addition, being able to identify SNPs involved in epistasis allows us to come up with an initial likely set of variants that are worth further exploration. Indeed, we advertise a two-step *ad hoc* epistasis association mapping procedure. First, we identify individual SNP associations with MAPIT. Then, we focus on the most significant associations from the first step to further test all of the pairwise interactions among them in order to identify specific epistatic interactions. Unlike the previous filtering strategies that are commonly used in epistatic mapping, our two-step procedure is unique in the sense that the SNP set identified in our first step contains SNPs that already display strong epistatic effects with other variants. Therefore, our two-step procedure outperforms alternative filtering strategies in simulations and real data applications. Nonetheless, we caution that the two-step procedure is still *ad hoc* in nature and could miss important epistatic associations. Therefore, exploring statistical approaches that can unify the two steps would be an interesting area for future research. Besides this main limitation, we also note that MAPIT

can be computationally expensive. MAPIT requires fitting a variance component model for every SNP in turn, and fitting variance component models are known to be computationally challenging [66, 68]. In this study, we use the recently developed MQS method for variance component estimation and testing. Compared with the standard REML method, MQS is computationally efficient, allows for exact p-value computation based on the Davies method, and is statistically more efficient than the REML estimates when the variance component is small [77]—a property that is particularly relevant here considering the marginal epistatic effect size is often small. MQS allows us to apply MAPIT to moderately sized genetic mapping studies with thousands of samples and millions of variants, which is otherwise impossible using any other variance component estimation methods. Still, new algorithms are likely needed to scale MAPIT up to datasets that orders of magnitude larger in size.

Supporting information

S1 Fig. Calibration of MAPIT p-values in the presence of population stratification effects. The QQ plots applying MAPIT to 100 simulated null datasets assuming sample sizes: 1,000 (A, D), 1,750 (B, E), and 2,500 (C, F). These results are based on using simulation model (ii). (A)-(C) use the top 5 genotype PCs, while (D)-(F) use the top 10 genotypes PCs. Blue dots are p-values produced by under the normal test (or z-test), while the black dots represent p-values tested using the Davies method via a mixture of chi-square distributions. The 95% confidence intervals for the null hypothesis of no association are shown in grey.
(PDF)

S2 Fig. Empirical power to detect simulated causal interacting makers and estimating their marginal PVE. Groups 1 and 2 causal markers are colored in light red and light blue, respectively. These figures are based on a broad-sense heritability level of $H^2 = 0.6$ and parameter $\rho = 0.5$, estimated with 100 replicates. Here, $\rho = 0.5$ was used to determine the portion of broad-sense heritability contributed by interaction effects. (A) shows the power of MAPIT to identify SNPs in each causal group under significance level $\alpha = 0.05$. The lines represent 95% variability due to resampling error. (B) shows boxplots of the marginal PVE estimates for the group 1 and 2 causal SNPs from MAPIT for the four simulation scenarios. The true PVEs per causal SNP (0.03 for the group 1 SNPs; 0.03, 0.015, 0.006, and 0.003 for the group 2 SNPs) are shown as dashed grey horizontal lines.
(PDF)

S3 Fig. Empirical power to detect simulated causal interacting makers and estimating their marginal PVE in the presence of population stratification effects (Top 5 PCs). Groups 1 and 2 causal markers are colored in light red and light blue, respectively. These figures are based on a broad-sense heritability level of $H^2 = 0.6$ and parameters $\rho = 0.5$ (A, B) and $\rho = 0.8$ (C, D), respectively. These results are estimated with 100 data replicates under simulation model (ii) with the top 5 genotype PCs. Here, $\rho = \{0.5, 0.8\}$ was used to determine the portion of broad-sense heritability contributed by interaction effects. (A) and (C) show the power of MAPIT to identify SNPs in each causal group under significance level $\alpha = 0.05$. The lines represent 95% variability due to resampling error. (B) and (D) show boxplots of the marginal PVE estimates for the group 1 and 2 causal SNPs from MAPIT for the four simulation scenarios. The true PVEs per causal SNP are shown as dashed grey horizontal lines. When $\rho = 0.05$, the true PVEs per causal SNP are: 0.03 for the group 1 SNPs; and 0.03, 0.015, 0.006, and 0.003 for the group 2 SNPs. When $\rho = 0.08$, the true PVEs per causal SNP are: 0.012 for the group 1 SNPs; and 0.012, 0.006, 0.0024, and 0.0012 for the Group 2 SNPs.
(PDF)

S4 Fig. Empirical power to detect simulated causal interacting makers and estimating their marginal PVE in the presence of population stratification effects (Top 10 PCs). Groups 1 and 2 causal markers are colored in light red and light blue, respectively. These figures are based on a broad-sense heritability level of $H^2 = 0.6$ and parameters $\rho = 0.5$ (A, B) and $\rho = 0.8$ (C, D), respectively. These results are estimated with 100 data replicates under simulation model (ii) with the top 10 genotype PCs. Here, $\rho = \{0.5, 0.8\}$ was used to determine the portion of broad-sense heritability contributed by interaction effects. (A) and (C) show the power of MAPIT to identify SNPs in each causal group under significance level $\alpha = 0.05$. The lines represent 95% variability due to resampling error. (B) and (D) show boxplots of the marginal PVE estimates for the group 1 and 2 causal SNPs from MAPIT for the four simulation scenarios. The true PVEs per causal SNP are shown as dashed grey horizontal lines. When $\rho = 0.05$, the true PVEs per causal SNP are: 0.03 for the group 1 SNPs; and 0.03, 0.015, 0.006, and 0.003 for the group 2 SNPs. When $\rho = 0.08$, the true PVEs per causal SNP are: 0.012 for the group 1 SNPs; and 0.012, 0.006, 0.0024, and 0.0012 for the Group 2 SNPs.
(PDF)

S5 Fig. Empirical power to detect simulated causal interacting makers. (A) and (B) show the power of MAPIT to identify SNPs in each causal group under the Bonferroni-corrected genome-wide significance level $\alpha = 8.3 \times 10^{-6}$. Groups 1 and 2 causal markers are colored in light red and light blue, respectively. These figures are based on a broad-sense heritability level of $H^2 = 0.6$, and parameters $\rho = 0.5$ (A) and $\rho = 0.8$ (B)—estimated with 100 replicates. Here, ρ was used to determine the portion of broad-sense heritability contributed by interaction effects. The lines represent 95% variability due to resampling error.
(PDF)

S6 Fig. Empirical power to detect simulated causal interacting makers in the presence of population stratification. All Figures show the power of MAPIT to identify SNPs in each causal group under the Bonferroni-corrected genome-wide significance level $\alpha = 8.3 \times 10^{-6}$. These results are estimated with 100 data replicates under simulation model (ii). (A) and (B) use the top 5 genotype PCs. (C) and (D) use the top 10 genotype PCs. Groups 1 and 2 causal markers are colored in light red and light blue, respectively. These figures are based on a broad-sense heritability level of $H^2 = 0.6$, and parameters $\rho = 0.5$ (A, C) and $\rho = 0.8$ (B, D). Here, ρ was used to determine the portion of broad-sense heritability contributed by interaction effects. The lines represent 95% variability due to resampling error.
(PDF)

S7 Fig. Accuracy of total pairwise epistatic PVE estimates across all simulation scenarios. Compared here are the epistatic PVE estimates computed by the standard variance component model. Each simulation scenario is represented by a different color, with each of the three simulation schemes being labeled on the x-axis. These figures are based on 100 simulations where the overall broad-sense heritability level is $H^2 = 0.6$, and the parameters $\rho = 0.5$ (A) and $\rho = 0.8$ (B). Here, ρ was used to determine the portion of broad-sense heritability contributed by interaction effects. In (A), the true epistatic PVE is 0.3. In (B), the true epistatic PVE is 0.12. In both cases, the true PVE is shown as the grey horizontal line.
(PDF)

S8 Fig. Power to detect pairwise epistatic heritability across all simulation scenarios. Compared here is the power of the standard variance component model to estimate the true non-zero pairwise epistatic PVE at the significance level of $\alpha = 0.05$ under a standard asymptotic normal test. Each simulation scenario is represented by a different color, with each of the three simulation schemes being labeled on the x-axis. These figures are based on 100 simulations

where the overall broad-sense heritability level is $H^2 = 0.6$, and the parameters $\rho = 0.5$ (A) and $\rho = 0.8$ (B). Here, ρ was used to determine the portion of broad-sense heritability contributed by interaction effects.
(PDF)

S9 Fig. Power analysis for detecting group 1 and group 2 causal SNPs. We compare the mapping abilities of MAPIT (solid line) to the exhaustive search procedure in PLINK (dotted line) in scenarios I (A), II (B), III (C), and IV (D), under broad-sense heritability level $H^2 = 0.6$ and $\rho = 0.5$. Here, $\rho = 0.5$ was used to determine the portion of broad-sense heritability contributed by interaction effects. Group 1 (light red) and group 2 (light blue) causal SNPs. The x-axis shows the false positive rate, while the y-axis gives the rate at which true causal variants were identified. Results are based on 100 replicates in each case.
(PDF)

S10 Fig. Power analysis for detecting group 1 and group 2 causal SNPs in the presence of population stratification effects (Top 5 PCs). We compare the mapping abilities of MAPIT (solid line) to the exhaustive search procedure in PLINK (dotted line) in scenarios I (A), II (B), III (C), and IV (D), under broad-sense heritability level $H^2 = 0.6$ and $\rho = 0.5$. Here, $\rho = 0.5$ was used to determine the portion of broad-sense heritability contributed by interaction effects. Group 1 (light red) and group 2 (light blue) causal SNPs. The x-axis shows the false positive rate, while the y-axis gives the rate at which true causal variants were identified. Results are based on 100 replicates in each case, where the data was created under simulation model (ii) with the top 5 genotype PCs.
(PDF)

S11 Fig. Power analysis for detecting group 1 and group 2 causal SNPs in the presence of population stratification effects (Top 5 PCs). We compare the mapping abilities of MAPIT (solid line) to the exhaustive search procedure in PLINK (dotted line) in scenarios I (A), II (B), III (C), and IV (D), under broad-sense heritability level $H^2 = 0.6$ and $\rho = 0.8$. Here, $\rho = 0.8$ was used to determine the portion of broad-sense heritability contributed by interaction effects. Group 1 (light red) and group 2 (light blue) causal SNPs. The x-axis shows the false positive rate, while the y-axis gives the rate at which true causal variants were identified. Results are based on 100 replicates in each case, where the data was created under simulation model (ii) with the top 5 genotype PCs.
(PDF)

S12 Fig. Power analysis for detecting group 1 and group 2 causal SNPs in the presence of population stratification effects (Top 10 PCs). We compare the mapping abilities of MAPIT (solid line) to the exhaustive search procedure in PLINK (dotted line) in scenarios I (A), II (B), III (C), and IV (D), under broad-sense heritability level $H^2 = 0.6$ and $\rho = 0.5$. Here, $\rho = 0.5$ was used to determine the portion of broad-sense heritability contributed by interaction effects. Group 1 (light red) and group 2 (light blue) causal SNPs. The x-axis shows the false positive rate, while the y-axis gives the rate at which true causal variants were identified. Results are based on 100 replicates in each case, where the data was created under simulation model (ii) with the top 10 genotype PCs.
(PDF)

S13 Fig. Power analysis for detecting group 1 and group 2 causal SNPs in the presence of population stratification effects (Top 10 PCs). We compare the mapping abilities of MAPIT (solid line) to the exhaustive search procedure in PLINK (dotted line) in scenarios I (A), II (B), III (C), and IV (D), under broad-sense heritability level $H^2 = 0.6$ and $\rho = 0.8$. Here, $\rho = 0.8$ was

used to determine the portion of broad-sense heritability contributed by interaction effects. Group 1 (light red) and group 2 (light blue) causal SNPs. The x-axis shows the false positive rate, while the y-axis gives the rate at which true causal variants were identified. Results are based on 100 replicates in each case, where the data was created under simulation model (ii) with the top 10 genotype PCs.
(PDF)

S14 Fig. Empirical power of exhaustive search procedures to detect epistatic pairs. Here, the effectiveness of MAPIT (green) as an initial step in a pairwise detection filtration process is compared against the more conventional single-SNP testing procedure, which is carried out via GEMMA (purple). In both cases, the search for epistatic pairs occurs between the top 100 significant marginally associated SNPs are considered. We use the fully exhaustive search model in PLINK (orange) as a baseline comparison. We compare the three methods in all scenarios (x-axis), under broad-sense heritability level $H^2 = 0.6$. Here, $\rho = 0.5$ was used to determine the portion of broad-sense heritability contributed by interaction effects. The y-axis gives the rate at which true causal epistatic pairs were identified. Results are based on 100 replicates in each case. The lines represent 95% variability due to resampling error.
(PDF)

S15 Fig. Empirical power of exhaustive search procedures to detect epistatic pairs in the presence of population stratification. Here, the effectiveness of MAPIT (green) as an initial step in a pairwise detection filtration process is compared against the more conventional single-SNP testing procedure, which is carried out via GEMMA (purple). In both cases, the search for epistatic pairs occurs between the top 100 significant marginally associated SNPs are considered. We use the fully exhaustive search model in PLINK (orange) as a baseline comparison. We compare the three methods in all scenarios (x-axis), under broad-sense heritability level $H^2 = 0.6$. Here, $\rho = 0.5$ (A, C) and $\rho = 0.8$ (B, D) were used to determine the portion of broad-sense heritability contributed by interaction effects. The y-axis gives the rate at which true causal epistatic pairs were identified. Results are based on 100 replicates in each case, where the data was created under simulation model (ii). (A) and (B) use the top 5 genotype PCs, while (C) and (D) use the top 10 genotypes PCs. The lines represent 95% variability due to resampling error.
(PDF)

S16 Fig. QQ-plots of the MAPIT p-values for all SNP-gene pairs in the GEUVADIS data set. (A) corresponds to using MAPIT with a genetic relatedness matrix $\mathbf{K}_{cis}$, where for the expression of each gene $\mathbf{K}_{cis}$ was computed using only the corresponding *cis*-SNPs. (B) corresponds to using MAPIT with a genetic relatedness matrix $\mathbf{K}_{trans}$, where for the expression of each gene $\mathbf{K}_{trans}$ was computed using SNPs outside of the corresponding *cis*-window. (C) corresponds to using MAPIT with a genome-wide genetic relatedness matrix $\mathbf{K}_{GW}$, where $\mathbf{K}_{GW}$ was computed using all SNPs in the study. (D) illustrates results from using MAPIT with $\mathbf{K}_{Pop}$, which was computed after we first controlled for residual population stratification effects.
(PDF)

S17 Fig. Comparison of epistatic filtration methods with MAPIT and GEMMA on the GEUVADIS data set. (A)-(C) show a histograms of the MAPIT p-values for all variants in the GEUVADIS data set using the genome-wide genetic relatedness matrix $\mathbf{K}_{trans}$ (A), $\mathbf{K}_{GW}$ (B), and $\mathbf{K}_{Pop}$ (C), respectively. The horizontal red line corresponds to a uniform distribution of p-values. (D)-(F) show the number of significant pairwise interactions (y-axis) identified by MAPIT (green) and GEMMA (purple) when searching between the top $v = \{1000, 2500, 5000, 7500, 10000, 15000, 20000\}$ marginally associated variants (x-axis). We use the number of

significant pairs identified by fully exhaustive search model in PLINK as a baseline comparison (orange dotted line). Note that PLINK only analyzes *cis*-SNPs pairs, while MAPIT with $\mathbf{K}_{trans}$ (D), $\mathbf{K}_{GW}$ (E), and $\mathbf{K}_{Pop}$ (F) effectively analyzes the marginal epistatic effects of *cis*-SNPs with all genome-wide SNPs. This image shows the distributions of genome-wide significant epistatic pairs as found by each method. An interaction for MAPIT and GEMMA was deemed signifiant if it had a joint p-value below the threshold $P = 0.05/(\sum_i q_i(q_i - 1)/2)$, where q_i is the number of top variants located in the *cis*-window of gene i. In the case of PLINK, we consider two variants to be a significantly associated epistatic pair if they have a joint p-value below the threshold $P = 1.09 \times 10^{-10}$, which corresponds to the Bonferroni-correction that would be used if we examined all possible genome-wide SNP pairs across all genes in the final data set. Overall, PLINK detected 7,361 (D, E), and 8,643 (F) significant pairwise interactions. (PDF)

S18 Fig. Enrichment of mepiQTL SNPs in GEUVADIS data set after using MAPIT with a genome-wide relatedness matrix. Shown here are the distribution of locations for significant SNPs, relative to the 5′ most gene transcription start site (TSS) and the 3′ most gene transcription end site (TES). (A) displays the marginally epistatic QTL (mepiQTL) detected by MAPIT using the genetic relatedness matrix $\mathbf{K}_{trans}$. (B) displays the marginally epistatic QTL (mepiQTL) detected by MAPIT using the genetic relatedness matrix $\mathbf{K}_{GW}$. (C) corresponds to the mepiQTL identified by MAPIT using $\mathbf{K}_{Pop}$. The x-axis of each plot divides a typical *cis*-candidate region into a series of bins. The y-axis plots the number of SNPs in each bin that have a p-value less than a gene specific Bonferroni-corrected significance p-value threshold $P = 0.05/\sum_i s_i$, where s_i is the number of *cis*-SNPs for gene i, divided by the total number of SNPs in that bin. Bars in green denote the region bounded by the TSS and TES, with gene lengths divided into 20 bins for visibility—because the gene body is thus artificially enlarged, SNP density within genes cannot be directly compared with SNP density outside of genes. (PDF)

S19 Fig. Chromosome-wide scans for epistatic effects in GEUVADIS data set. Depicted are the $-\log_{10}(P)$ transformed MAPIT p-values of quality-control-positive *cis*-SNPs plotted against their genomic position in chromosomes (A) 2, (B) 3, and (C) 4, respectively. Note that MAPIT was implemented with $\mathbf{K}_{cis}$. Here, the epistatic associated genes are labeled (blue). The (red) horizontal line indicates a genome-wide significance threshold ($P = 1.828 \times 10^{-8}$). Note that all panels are truncated at $-\log_{10}(P) = 10$ for consistency and presentation, although for some genes there are strongly marginally epistatic associated markers with p-values $P \approx 0$. (PDF)

S20 Fig. Chromosome-wide scans for epistatic effects in GEUVADIS data set. Depicted are the $-\log_{10}(P)$ transformed MAPIT p-values of quality-control-positive *cis*-SNPs plotted against their genomic position in chromosomes (A) 5, (B) 7, and (C) 8, respectively. Note that MAPIT was implemented with $\mathbf{K}_{cis}$. Here, the epistatic associated genes are labeled (blue). The (red) horizontal line indicates a genome-wide significance threshold ($P = 1.828 \times 10^{-8}$). Note that all panels are truncated at $-\log_{10}(P) = 10$ for consistency and presentation, although for some genes there are strongly marginally epistatic associated markers with p-values $P \approx 0$. (PDF)

S21 Fig. Chromosome-wide scans for epistatic effects in GEUVADIS data set. Depicted are the $-\log_{10}(P)$ transformed MAPIT p-values of quality-control-positive *cis*-SNPs plotted against their genomic position in chromosomes (A) 9, (B) 10, and (C) 11, respectively. Note that MAPIT was implemented with $\mathbf{K}_{cis}$. Here, the epistatic associated genes are labeled (blue). The (red) horizontal line indicates a genome-wide significance threshold ($P = 1.828 \times 10^{-8}$). Note

that all panels are truncated at $-\log_{10}(P) = 10$ for consistency and presentation, although for some genes there are strongly marginally epistatic associated markers with p-values $P \approx 0$.
(PDF)

S22 Fig. Chromosome-wide scans for epistatic effects in GEUVADIS data set. Depicted are the $-\log_{10}(P)$ transformed MAPIT p-values of quality-control-positive *cis*-SNPs plotted against their genomic position in chromosomes (A) 12, (B) 13, and (C) 14, respectively. Note that MAPIT was implemented with $\mathbf{K}_{cis}$. Here, the epistatic associated genes are labeled (blue). The (red) horizontal line indicates a genome-wide significance threshold ($P = 1.828 \times 10^{-8}$). Note that all panels are truncated at $-\log_{10}(P) = 10$ for consistency and presentation, although for some genes there are strongly marginally epistatic associated markers with p-values $P \approx 0$.
(PDF)

S23 Fig. Chromosome-wide scans for epistatic effects in GEUVADIS data set. Depicted are the $-\log_{10}(P)$ transformed MAPIT p-values of quality-control-positive *cis*-SNPs plotted against their genomic position in chromosomes (A) 15, (B) 16, and (C) 17, respectively. Note that MAPIT was implemented with $\mathbf{K}_{cis}$. Here, the epistatic associated genes are labeled (blue). The (red) horizontal line indicates a genome-wide significance threshold ($P = 1.828 \times 10^{-8}$). Note that all panels are truncated at $-\log_{10}(P) = 10$ for consistency and presentation, although for some genes there are strongly marginally epistatic associated markers with p-values $P \approx 0$.
(PDF)

S24 Fig. Chromosome-wide scans for epistatic effects in GEUVADIS data set. Depicted are the $-\log_{10}(P)$ transformed MAPIT p-values of quality-control-positive *cis*-SNPs plotted against their genomic position in chromosomes (A) 18, (B) 19, (C) 20, and (D) 21 respectively. Note that MAPIT was implemented with $\mathbf{K}_{cis}$. Here, the epistatic associated genes are labeled (blue). The (red) horizontal line indicates a genome-wide significance threshold ($P = 1.828 \times 10^{-8}$). Note that all panels are truncated at $-\log_{10}(P) = 10$ for consistency and presentation, although for some genes there are strongly marginally epistatic associated markers with p-values $P \approx 0$.
(PDF)

S25 Fig. Estimates of the proportion of phenotypic variance explained (PVE) by additive and pairwise epistatic effects for each gene analyzed in the GEUVADIS data set. Estimates of the pPVE on the y-axis were calculated by using variance component models, where each of the components represent for additive effects (grey) and pairwise epistasis (green). More specifically, the variance components correspond to additive and pairwise epistatic covariance matrices $\mathbf{K}$ and $\mathbf{K}^2$, respectively. Note that $\mathbf{K}^2 = \mathbf{K} \circ \mathbf{K}$ is obtained by using the Hadamard product (i.e. the squaring of each element) of the matrix $\mathbf{K}$. See Methods and Material for details.
(PDF)

S1 Table. Computational complexity for running MAPIT as a function of sample size and the number of SNPs. Each entry represents the mean computation time (in minutes) it takes to run MAPIT under different hypothesis testing strategies. These tests are the normal test, and the Davies method for approximating a mixture of chi-squares. Computations were performed using 32 cores on Duke University's Center for Genomic and Computational Biology HARDAC Cluster. To create genetic data for these simulations, we generated 5×10^3, 1×10^4, 5×10^4, and 1×10^5 genetic markers, respectively. Sample sizes were set to 1,000, 2,500, and 5,000. Values in the parentheses are the standard deviations of the estimates.
(PDF)

S2 Table. Empirical type I error estimates of MAPIT in the presence of population stratification effects (Top 5 PCs). Each entry represents type I error rate estimates as the proportion of p-values a under the null hypothesis based on 100 simulated continuous phenotypes for the normal test (or z-test) and the Davies method. These results are based on 100 simulated data sets using simulation model (ii) with the top 5 genotype PCs. Recall that model (ii) is used to evaluate the type I error control of MAPIT when there is population stratification. Empirical size for the analyses used significance thresholds of $\alpha = 0.05, 0.01$, and 0.001. Sample sizes were set to 1,000, 1,750, and 2,500. Values in the parentheses are the standard deviations of the estimates.
(PDF)

S3 Table. Empirical type I error estimates of MAPIT in the presence of population stratification effects (Top 10 PCs). Each entry represents type I error rate estimates as the proportion of p-values a under the null hypothesis based on 100 simulated continuous phenotypes for the normal test (or z-test) and the Davies method. These results are based on 100 simulated data sets using simulation model (ii) with the top 10 genotype PCs. Recall that model (ii) is used to evaluate the type I error control of MAPIT when there is population stratification. Empirical size for the analyses used significance thresholds of $\alpha = 0.05, 0.01$, and 0.001. Sample sizes were set to 1,000, 1,750, and 2,500. Values in the parentheses are the standard deviations of the estimates.
(PDF)

S4 Table. Percentage of overlap (i.e. coverage) between the mepiQTL detected by MAPIT, the eQTL identified by GEMMA, and the epiQTL found by PLINK. Coverage was computed as the proportion of significant QTL detected by row j that were also identified by column k.
(XLSX)

S5 Table. Percentage of overlap (i.e. coverage) between the mepiGenes detected by MAPIT, the eGenes identified by GEMMA, and the epiGenes found by PLINK. Coverage was computed as the proportion of significant genes detected by row j that were also identified by column k.
(XLSX)

S6 Table. The marginal epistatic p-values for all significant mepiQTL as computed by MAPIT in the GEUVADIS data set using the _cis_-gene specific genetic relatedness matrix $\mathbf{K}_{cis}$. Strong significance of association for a particular SNP or locus was determined by using a gene specific Bonferroni-corrected significance p-value threshold $P = 0.05/\sum_i s_i$, where s_i is the number of _cis_-SNPs for gene i. Also listed are the corresponding genes whose expressions are associated.
(XLSX)

S7 Table. The marginal epistatic p-values for all significant mepiQTL as computed by MAPIT in the GEUVADIS data set using the _cis_-gene specific genetic relatedness matrix $\mathbf{K}_{trans}$. Strong significance of association for a particular SNP or locus was determined by using a gene specific Bonferroni-corrected significance p-value threshold $P = 0.05/\sum_i s_i$, where s_i is the number of _cis_-SNPs for gene i. Also listed are the corresponding genes whose expressions are associated.
(XLSX)

S8 Table. The marginal epistatic p-values for all significant mepiQTL as computed by MAPIT in the GEUVADIS data set using the genome-wide specific genetic relatedness matrix $\mathbf{K}_{GW}$. Strong significance of association for a particular SNP or locus was determined

by using a gene specific Bonferroni-corrected significance p-value threshold $P = 0.05/\sum_i s_i$, where s_i is the number of *cis*-SNPs for gene *i*. Also listed are the corresponding genes whose expressions are associated.
(XLSX)

S9 Table. The marginal epistatic p-values for all significant mepiQTL as computed by MAPIT in the GEUVADIS data set using the genome-wide specific genetic relatedness matrix K_{Pop}. Strong significance of association for a particular SNP or locus was determined by using a gene specific Bonferroni-corrected significance p-value threshold $P = 0.05/\sum_i s_i$, where s_i is the number of *cis*-SNPs for gene *i*. Also listed are the corresponding genes whose expressions are associated.
(XLSX)

Acknowledgments

We thank Kris C. Wood for helpful comments on a previous version of the manuscript. This study also makes use of data generated by the Wellcome Trust Case Control Consortium (WTCCC). A full list of the investigators who contributed to the generation of the data is available from www.wtccc.org.uk.

Author Contributions

Conceptualization: Lorin Crawford, Sayan Mukherjee, Xiang Zhou.

Data curation: Lorin Crawford, Ping Zeng, Xiang Zhou.

Formal analysis: Lorin Crawford, Xiang Zhou.

Funding acquisition: Lorin Crawford, Sayan Mukherjee, Xiang Zhou.

Investigation: Lorin Crawford, Ping Zeng, Xiang Zhou.

Methodology: Lorin Crawford, Xiang Zhou.

Project administration: Lorin Crawford, Sayan Mukherjee, Xiang Zhou.

Resources: Lorin Crawford, Sayan Mukherjee, Xiang Zhou.

Software: Lorin Crawford, Xiang Zhou.

Supervision: Lorin Crawford, Sayan Mukherjee, Xiang Zhou.

Validation: Lorin Crawford, Xiang Zhou.

Visualization: Lorin Crawford, Sayan Mukherjee, Xiang Zhou.

Writing – original draft: Lorin Crawford, Ping Zeng, Sayan Mukherjee, Xiang Zhou.

Writing – review & editing: Lorin Crawford, Ping Zeng, Sayan Mukherjee, Xiang Zhou.

References

1. Visscher PM, Brown MA, McCarthy MI, Yang J. Five Years of GWAS Discovery. The American Journal of Human Genetics. 2012 1; 90(1):7–24. Available from: http://www.ncbi.nlm.nih.gov/pmc/articles/PMC3257326/. https://doi.org/10.1016/j.ajhg.2011.11.029 PMID: 22243964

2. Pickrell JK, Marioni JC, Pai AA, Degner JF, Engelhardt BE, Nkadori E, et al. Understanding mechanisms underlying human gene expression variation with RNA sequencing. Nature. 2010 4; 464(7289): 768–772. Available from: http://dx.doi.org/10.1038/nature08872. PMID: 20220758

3. Battle A, Mostafavi S, Zhu X, Potash JB, Weissman MM, McCormick C, et al. Characterizing the genetic basis of transcriptome diversity through RNA-sequencing of 922 individuals. Genome

Research. 2013 10; Available from: http://genome.cshlp.org/content/early/2013/10/02/gr.155192.113.abstract.

4. Lappalainen T, Sammeth M, Friedlander MR, 't Hoen PAC, Monlong J, Rivas MA, et al. Transcriptome and genome sequencing uncovers functional variation in humans. Nature. 2013 9; 501(7468):506–511. Available from: http://dx.doi.org/10.1038/nature12531. PMID: 24037378

5. Tung J, Zhou X, Alberts SC, Stephens M, Gilad Y. The genetic architecture of gene expression levels in wild baboons. eLife. 2015; 4:e04729. Available from: http://www.ncbi.nlm.nih.gov/pmc/articles/PMC4383332/. https://doi.org/10.7554/eLife.04729

6. Phillips PC. Epistasis—the essential role of gene interactions in the structure and evolution of genetic systems. Nat Rev Genet. 2008 10; 9(11):855–867. Available from: http://www.ncbi.nlm.nih.gov/pmc/articles/PMC2689140/. https://doi.org/10.1038/nrg2452 PMID: 18852697

7. Mackay TFC. Epistasis and quantitative traits: using model organisms to study gene-gene interactions. Nat Rev Genet. 2014 1; 15(1):22–33. Available from: http://dx.doi.org/10.1038/nrg3627. PMID: 24296533

8. Carlborg O, Jacobsson L, Ahgren P, Siegel P, Andersson L. Epistasis and the release of genetic variation during long-term selection. Nat Genet. 2006 4; 38(4):418–420. Available from: http://dx.doi.org/10.1038/ng1761. PMID: 16532011

9. Martin G, Elena SF, Lenormand T. Distributions of epistasis in microbes fit predictions from a fitness landscape model. Nat Genet. 2007; 39:555–560. https://doi.org/10.1038/ng1998 PMID: 17369829

10. Bloom JS, Ehrenreich IM, Loo WT, Lite TLV, Kruglyak L. Finding the sources of missing heritability in a yeast cross. Nature. 2013 2; 494(7436):234–237. Available from: http://dx.doi.org/10.1038/nature11867. PMID: 23376951

11. Shao H, Burrage LC, Sinasac DS, Hill AE, Ernest SR, O'Brien W, et al. Genetic architecture of complex traits: Large phenotypic effects and pervasive epistasis. Proceedings of the National Academy of Sciences. 2008 12; 105(50):19910–19914. Available from: http://www.pnas.org/content/105/50/19910.abstract. https://doi.org/10.1073/pnas.0810388105

12. He X, Qian W, Wang Z, Li Y, Zhang J. Prevalent positive epistasis in Escherichia coli and Saccharomyces cerevisiae metabolic networks. Nat Genet. 2010 3; 42(3):272–276. Available from: http://dx.doi.org/10.1038/ng.524. PMID: 20101242

13. Chari S, Dworkin I. The Conditional Nature of Genetic Interactions: The Consequences of Wild-Type Backgrounds on Mutational Interactions in a Genome-Wide Modifier Screen. PLoS Genet. 2013 8; 9(8):e1003661. Available from: http://dx.doi.org/10.1371%2Fjournal.pgen.1003661. PMID: 23935530

14. Monnahan PJ, Kelly JK. Epistasis Is a Major Determinant of the Additive Genetic Variance in *Mimulus guttatus*. PLoS Genet. 2015 5; 11(5):e1005201. Available from: http://dx.doi.org/10.1371%2Fjournal.pgen.1005201. PMID: 25946702

15. Collins SR, Schuldiner M, Krogan NJ, Weissman JS. A strategy for extracting and analyzing large-scale quantitative epistatic interaction data. Genome Biology. 2006; 7(7):R63. Available from: http://dx.doi.org/10.1186/gb-2006-7-7-r63. PMID: 16859555

16. Costanzo M, Baryshnikova A, Bellay J, Kim Y, Spear ED, Sevier CS, et al. The Genetic Landscape of a Cell. Science. 2010 1; 327(5964):425. Available from: http://science.sciencemag.org/content/327/5964/425.abstract. https://doi.org/10.1126/science.1180823 PMID: 20093466

17. Horn T, Sandmann T, Fischer B, Axelsson E, Huber W, Boutros M. Mapping of signaling networks through synthetic genetic interaction analysis by RNAi. Nat Meth. 2011 4; 8(4):341–346. Available from: http://dx.doi.org/10.1038/nmeth.1581.

18. Lehner B, Crombie C, Tischler J, Fortunato A, Fraser AG. Systematic mapping of genetic interactions in Caenorhabditis elegans identifies common modifiers of diverse signaling pathways. Nat Genet. 2006 8; 38(8):896–903. Available from: http://dx.doi.org/10.1038/ng1844. PMID: 16845399

19. Szappanos B, Kovacs K, Szamecz B, Honti F, Costanzo M, Baryshnikova A, et al. An integrated approach to characterize genetic interaction networks in yeast metabolism. Nat Genet. 2011 7; 43(7):656–662. Available from: http://dx.doi.org/10.1038/ng.846. PMID: 21623372

20. Tong AHY, Lesage G, Bader GD, Ding H, Xu H, Xin X, et al. Global Mapping of the Yeast Genetic Interaction Network. Science. 2004 2; 303(5659):808. Available from: http://science.sciencemag.org/content/303/5659/808.abstract. https://doi.org/10.1126/science.1091317 PMID: 14764870

21. Onge RPS, Mani R, Oh J, Proctor M, Fung E, Davis RW, et al. Systematic pathway analysis using high-resolution fitness profiling of combinatorial gene deletions. Nat Genet. 2007 2; 39(2):199–206. Available from: http://dx.doi.org/10.1038/ng1948.

22. Deutschbauer AM, Davis RW. Quantitative trait loci mapped to single-nucleotide resolution in yeast. Nat Genet. 2005 12; 37(12):1333–1340. Available from: http://dx.doi.org/10.1038/ng1674. PMID: 16273108

23. Gerke J, Lorenz K, Cohen B. Genetic Interactions Between Transcription Factors Cause Natural Variation in Yeast. Science. 2009 1; 323(5913):498. Available from: http://science.sciencemag.org/content/323/5913/498.abstract. https://doi.org/10.1126/science.1166426 PMID: 19164747

24. Brem RB, Storey JD, Whittle J, Kruglyak L. Genetic interactions between polymorphisms that a ect gene expression in yeast. Nature. 2005 8; 436(7051):701–703. Available from: http://dx.doi.org/10.1038/nature03865. PMID: 16079846

25. Gaertner BE, Parmenter MD, Rockman MV, Kruglyak L, Phillips PC. More Than the Sum of Its Parts: A Complex Epistatic Network Underlies Natural Variation in Thermal Preference Behavior in *Caenorhabditis elegans*. Genetics. 2012 12; 192(4):1533. Available from: http://www.genetics.org/content/192/4/1533.abstract. https://doi.org/10.1534/genetics.112.142877 PMID: 23086219

26. Flint J, Mackay TFC. Genetic architecture of quantitative traits in mice, flies, and humans. Genome Research. 2009 5; 19(5):723–733. Available from: http://genome.cshlp.org/content/19/5/723.abstract. https://doi.org/10.1101/gr.086660.108 PMID: 19411597

27. Jarvis JP, Cheverud JM. Mapping the Epistatic Network Underlying Murine Reproductive Fatpad Variation. Genetics. 2011 2; 187(2):597. Available from: http://www.genetics.org/content/187/2/597.abstract. https://doi.org/10.1534/genetics.110.123505 PMID: 21115969

28. Leamy L, Gordon R, Pomp D. Sex-, Diet-, and Cancer-Dependent Epistatic Effects on Complex Traits in Mice. Frontiers in Genetics. 2011; 2:71. Available from: http://journal.frontiersin.org/article/10.3389/fgene.2011.00071. PMID: 22303366

29. Peripato A, De Brito R, Matioli S, Pletscher L, Vaughn T, Cheverud J. Epistasis a ecting litter size in mice. Journal of Evolutionary Biology. 2004; 17(3):593–602. https://doi.org/10.1111/j.1420-9101.2004.00702.x PMID: 15149402

30. Pettersson M, Besnier F, Siegel PB, Carlborg Ö. Replication and explorations of high-order epistasis using a large advanced intercross line pedigree. PLoS Genet. 2011; 7(7):e1002180. https://doi.org/10.1371/journal.pgen.1002180 PMID: 21814519

31. Kroymann J, Mitchell-Olds T. Epistasis and balanced polymorphism influencing complex trait variation. Nature. 2005; 435(7038):95–98. https://doi.org/10.1038/nature03480 PMID: 15875023

32. Rowe HC, Hansen BG, Halkier BA, Kliebenstein DJ. Biochemical networks and epistasis shape the Arabidopsis thaliana metabolome. The Plant Cell. 2008; 20(5):1199–1216. https://doi.org/10.1105/tpc.108.058131 PMID: 18515501

33. Wentzell AM, Rowe HC, Hansen BG, Ticconi C, Halkier BA, Kliebenstein DJ. Linking metabolic QTLs with network and cis-eQTLs controlling biosynthetic pathways. PLoS Genet. 2007; 3(9):e162. https://doi.org/10.1371/journal.pgen.0030162

34. Hill WG, Goddard ME, Visscher PM. Data and Theory Point to Mainly Additive Genetic Variance for Complex Traits. PLoS Genet. 2008 2; 4(2):e1000008. Available from: http://dx.doi.org/10.1371%2Fjournal.pgen.1000008. PMID: 18454194

35. Mäki-Tanila A, Hill WG. Influence of Gene Interaction on Complex Trait Variation with Multilocus Models. Genetics. 2014 9; 198(1):355. Available from: http://www.genetics.org/content/198/1/355.abstract. https://doi.org/10.1534/genetics.114.165282

36. Huang W, Mackay TFC. The Genetic Architecture of Quantitative Traits Cannot Be Inferred from Variance Component Analysis. PLOS Genetics. 2016 11; 12(11):e1006421. Available from: http://dx.doi.org/10.1371%2Fjournal.pgen.1006421. PMID: 27812106

37. Brown AA, Buil A, Viñuela A, Lappalainen T, Zheng HF, Richards JB, et al. Genetic interactions a ecting human gene expression identified by variance association mapping. eLife. 2014; 3:e01381. Available from: https://dx.doi.org/10.7554/eLife.01381. PMID: 24771767

38. The Wellcome Trust Case Control Consortium 2 G. A genome-wide association study identifies new psoriasis susceptibility loci and an interaction between HLA-C and ERAP1. Nat Genet. 2010 11; 42(11):985–990. Available from: http://dx.doi.org/10.1038/ng.694.

39. Hemani G, Shakhbazov K, Westra HJ, Esko T, Henders AK, McRae AF, et al. Detection and replication of epistasis influencing transcription in humans. Nature. 2014 4; 508(7495):249–253. Available from: http://dx.doi.org/10.1038/nature13005. PMID: 24572353

40. Evans DM, Spencer CCA, Pointon JJ, Su Z, Harvey D, Kochan G, et al. Interaction between ERAP1 and HLA-B27 in ankylosing spondylitis implicates peptide handling in the mechanism for HLA-B27 in disease susceptibility. Nat Genet. 2011 8; 43(8):761–767. Available from: http://dx.doi.org/10.1038/ng.873. PMID: 21743469

41. Wood AR, Tuke MA, Nalls MA, Hernandez DG, Bandinelli S, Singleton AB, et al. Another explanation for apparent epistasis. Nature. 2014; 514(7520):E3–E5. https://doi.org/10.1038/nature13691 PMID: 25279928

42. Crow JF. On epistasis: why it is unimportant in polygenic directional selection. Philosophical Transactions of the Royal Society B: Biological Sciences. 2010 3; 365(1544):1241. Available from: http://rstb.royalsocietypublishing.org/content/365/1544/1241.abstract. https://doi.org/10.1098/rstb.2009.0275

43. Forsberg SKG, Bloom JS, Sadhu MJ, Kruglyak L, Carlborg O. Accounting for genetic interactions improves modeling of individual quantitative trait phenotypes in yeast. Nat Genet. 2017 2; advance online publication:-. Available from: http://dx.doi.org/10.1038/ng.3800. PMID: 28250458

44. Jiang Y, Reif JC. Modeling Epistasis in Genomic Selection. Genetics. 2015 10; 201(2):759–768. Available from: http://www.genetics.org/content/201/2/759.abstract. https://doi.org/10.1534/genetics.115.177907

45. Muñoz PR, Resende MFR, Gezan SA, Resende MDV, de los Campos G, Kirst M, et al. Unraveling Additive from Non-Additive Effects Using Genomic Relationship Matrices. Genetics. 2014 10; Available from: http://www.genetics.org/content/early/2014/10/15/genetics.114.171322.abstract.

46. Aschard H, Chen J, Cornelis MC, Chibnik LB, Karlson EW, Kraft P. Inclusion of Gene-Gene and Gene-Environment Interactions Unlikely to Dramatically Improve Risk Prediction for Complex Diseases. American Journal of Human Genetics. 2012 6; 90(6):962–972. Available from: http://www.ncbi.nlm.nih.gov/pmc/articles/PMC3370279/. https://doi.org/10.1016/j.ajhg.2012.04.017 PMID: 22633398

47. Eichler EE, Flint J, Gibson G, Kong A, Leal SM, Moore JH, et al. Missing heritability and strategies for finding the underlying causes of complex disease. Nat Rev Genet. 2010 6; 11(6):446–450. Available from: http://dx.doi.org/10.1038/nrg2809. PMID: 20479774

48. Hemani G, Knott S, Haley C. An Evolutionary Perspective on Epistasis and the Missing Heritability. PLoS Genet. 2013 2; 9(2):e1003295. Available from: http://dx.doi.org/10.1371%2Fjournal.pgen.1003295. PMID: 23509438

49. Zuk O, Hechter E, Sunyaev SR, Lander ES. The mystery of missing heritability: Genetic interactions create phantom heritability. Proceedings of the National Academy of Sciences. 2012 1; 109(4):1193–1198. Available from: http://www.pnas.org/content/109/4/1193.abstract. https://doi.org/10.1073/pnas.1119675109

50. Yang J, Bakshi A, Zhu Z, Hemani G, Vinkhuyzen AAE, Lee SH, et al. Genetic variance estimation with imputed variants finds negligible missing heritability for human height and body mass index. Nat Genet. 2015 10; 47(10):1114–1120. Available from: http://dx.doi.org/10.1038/ng.3390. PMID: 26323059

51. Wei WH, Hemani G, Haley CS. Detecting epistasis in human complex traits. Nat Rev Genet. 2014 11; 15(11):722–733. Available from: http://dx.doi.org/10.1038/nrg3747. PMID: 25200660

52. Cordell HJ. Detecting gene-gene interactions that underlie human diseases. Nat Rev Genet. 2009 6; 10(6):392–404. Available from: http://dx.doi.org/10.1038/nrg2579. PMID: 19434077

53. Ma L, Clark AG, Keinan A. Gene-Based Testing of Interactions in Association Studies of Quantitative Traits. PLoS Genet. 2013 2; 9(2):e1003321. Available from: http://dx.doi.org/10.1371%2Fjournal.pgen.1003321. PMID: 23468652

54. Zhang X, Huang S, Zou F, Wang W. TEAM: efficient two-locus epistasis tests in human genome-wide association study. Bioinformatics. 2010 6; 26(12):217–227. Available from: http://bioinformatics.oxfordjournals.org/content/26/12/i217.abstract. https://doi.org/10.1093/bioinformatics/btq186

55. Lippert C, Listgarten J, Davidson RI, Baxter J, Poon H, Kadie CM, et al. An Exhaustive Epistatic SNP Association Analysis on Expanded Wellcome Trust Data. Scientific Reports. 2013 1; 3:1099 EP—. Available from: http://dx.doi.org/10.1038/srep01099. PMID: 23346356

56. Hemani G, Theocharidis A, Wei W, Haley C. EpiGPU: exhaustive pairwise epistasis scans parallelized on consumer level graphics cards. Bioinformatics. 2011 6; 27(11):1462–1465. https://doi.org/10.1093/bioinformatics/btr172 PMID: 21471009

57. Prabhu S, Pe'er I. Ultrafast genome-wide scan for SNP-SNP interactions in common complex disease. Genome Research. 2012 11; 22(11):2230–2240. Available from: http://www.ncbi.nlm.nih.gov/pmc/articles/PMC3483552/. https://doi.org/10.1101/gr.137885.112 PMID: 22767386

58. Lewinger JP, Morrison JL, Thomas DC, Murcray CE, Conti DV, Li D, et al. Efficient two-step testing of gene-gene interactions in genome-wide association studies. Genetic Epidemiology. 2013 7; 37(5):440–451. https://doi.org/10.1002/gepi.21720 PMID: 23633124

59. Ueki M, Cordell HJ. Improved Statistics for Genome-Wide Interaction Analysis. PLoS Genet. 2012 4; 8(4):e1002625. Available from: http://dx.doi.org/10.1371%2Fjournal.pgen.1002625. PMID: 22496670

60. Zhang Y, Liu JS. Bayesian inference of epistatic interactions in case-control studies. Nat Genet. 2007 9; 39(9):1167–1173. Available from: http://dx.doi.org/10.1038/ng2110. PMID: 17721534

61. Tang W, Wu X, Jiang R, Li Y. Epistatic Module Detection for Case-Control Studies: A Bayesian Model with a Gibbs Sampling Strategy. PLoS Genet. 2009 5; 5(5):e1000464. Available from: http://dx.doi.org/10.1371%2Fjournal.pgen.1000464. PMID: 19412524

62. Zhang Y, Zhang J, Liu JS. Block-based Bayesian epistasis association mapping with application to WTCCC type 1 diabetes data. Annals of Applied Statistics. 2011; 5(3):2052–2077. Available from: http://projecteuclid.org/euclid.aoas/1318514295. https://doi.org/10.1214/11-AOAS469 PMID: 22140419

63. Wan X, Yang C, Yang Q, Xue H, Fan X, Tang NLS, et al. BOOST: A Fast Approach to Detecting Gene-Gene Interactions in Genome-wide Case-Control Studies. The American Journal of Human Genetics. 2010 9; 87(3):325–340. Available from: http://www.sciencedirect.com/science/article/pii/S0002929710003782. https://doi.org/10.1016/j.ajhg.2010.07.021 PMID: 20817139

64. Wu MC, Lee S, Cai T, Li Y, Boehnke M, Lin X. Rare-Variant Association Testing for Sequencing Data with the Sequence Kernel Association Test. The American Journal of Human Genetics. 2011 7; 89(1): 82–93. Available from: http://www.ncbi.nlm.nih.gov/pmc/articles/PMC3135811/. https://doi.org/10.1016/j.ajhg.2011.05.029 PMID: 21737059

65. Lee S, Wu MC, Lin X. Optimal tests for rare variant effects in sequencing association studies. Biostatistics (Oxford, England). 2012 9; 13(4):762–775. Available from: http://www.ncbi.nlm.nih.gov/pmc/articles/PMC3440237/. https://doi.org/10.1093/biostatistics/kxs014

66. Zhou X, Stephens M. Genome-wide Efficient Mixed Model Analysis for Association Studies. Nat Genet. 2012 7; 44(7):821–824. Available from: http://www.ncbi.nlm.nih.gov/pmc/articles/PMC3386377/. https://doi.org/10.1038/ng.2310 PMID: 22706312

67. Zhou X, Carbonetto P, Stephens M. Polygenic Modeling with Bayesian Sparse Linear Mixed Models. PLoS Genet. 2013 2; 9(2):e1003264. Available from: http://dx.doi.org/10.1371%2Fjournal.pgen.1003264. PMID: 23408905

68. Zhou X, Stephens M. Efficient multivariate linear mixed model algorithms for genome-wide association studies. Nat Meth. 2014 4; 11(4):407–409. Available from: http://dx.doi.org/10.1038/nmeth.2848.

69. Yang J, Benyamin B, McEvoy BP, Gordon S, Henders AK, Nyholt DR, et al. Common SNPs explain a large proportion of the heritability for human height. Nat Genet. 2010 7; 42(7):565–569. Available from: http://dx.doi.org/10.1038/ng.608. PMID: 20562875

70. Kang HM, Sul JH, Service SK, Zaitlen NA, Kong Sy, Freimer NB, et al. Variance component model to account for sample structure in genome-wide association studies. Nat Genet. 2010 4; 42(4):348–354. Available from: http://dx.doi.org/10.1038/ng.548. PMID: 20208533

71. Lippert C, Listgarten J, Liu Y, Kadie CM, Davidson RI, Heckerman D. FaST linear mixed models for genome-wide association studies. Nat Meth. 2011 10; 8(10):833–835. Available from: http://dx.doi.org/10.1038/nmeth.1681.

72. Yu J, Pressoir G, Briggs WH, Vroh Bi I, Yamasaki M, Doebley JF, et al. A unified mixed-model method for association mapping that accounts for multiple levels of relatedness. Nat Genet. 2006 2; 38(2): 203–208. Available from: http://dx.doi.org/10.1038/ng1702. PMID: 16380716

73. Zhang Z, Ersoz E, Lai CQ, Todhunter RJ, Tiwari HK, Gore MA, et al. Mixed linear model approach adapted for genome-wide association studies. Nat Genet. 2010 4; 42(4):355–360. Available from: http://dx.doi.org/10.1038/ng.546. PMID: 20208535

74. Korte A, Vilhjalmsson BJ, Segura V, Platt A, Long Q, Nordborg M. A mixed-model approach for genome-wide association studies of correlated traits in structured populations. Nat Genet. 2012 9; 44(9):1066–1071. Available from: http://dx.doi.org/10.1038/ng.2376. PMID: 22902788

75. Speed D, Hemani G, Johnson MR, Balding DJ. Improved Heritability Estimation from Genome-wide SNPs. The American Journal of Human Genetics. 2012 2017/2/26; 91(6):1011–1021. Available from: http://dx.doi.org/10.1016/j.ajhg.2012.10.010.

76. Yang J, Zaitlen NA, Goddard ME, Visscher PM, Price AL. Advantages and pitfalls in the application of mixed-model association methods. Nat Genet. 2014 2; 46(2):100–106. Available from: http://dx.doi.org/10.1038/ng.2876. PMID: 24473328

77. Zhou X. A Unified Framework for Variance Component Estimation with Summary Statistics in Genome-wide Association Studies. Annals of Applied Statistics. 2017; Available from: http://biorxiv.org/content/early/2016/03/08/042846.abstract.

78. Haseman JK, Elston RC. The investigation of linkage between a quantitative trait and a marker locus. Behavior Genetics. 1972; 2(1):3–19. Available from: http://dx.doi.org/10.1007/BF01066731. PMID: 4157472

79. Golan D, Lander ES, Rosset S. Measuring missing heritability: Inferring the contribution of common variants. Proceedings of the National Academy of Sciences. 2014 12; 111(49):E5272–E5281. Available from: http://www.pnas.org/content/111/49/E5272.abstract. https://doi.org/10.1073/pnas.1419064111

80. Churchill GA, Doerge RW. Naive Application of Permutation Testing Leads to Inflated Type I Error Rates. Genetics. 2008 1; 178(1):609–610. Available from: http://www.genetics.org/content/178/1/609.abstract. https://doi.org/10.1534/genetics.107.074609 PMID: 18202402

81. Davies RB. Algorithm AS 155: The Distribution of a Linear Combination of $\sim^2$ Random Variables. Journal of the Royal Statistical Society Series C (Applied Statistics). 1980; 29(3):323–333. Available from: http://www.jstor.org/stable/2346911.

82. Purcell S, Neale B, Todd-Brown K, Thomas L, Ferreira MAR, Bender D, et al. PLINK: A Tool Set for Whole-Genome Association and Population-Based Linkage Analyses. The American Journal of Human Genetics. 2007 9; 81(3):559–575. Available from: http://www.sciencedirect.com/science/article/pii/S0002929707613524. https://doi.org/10.1086/519795 PMID: 17701901

83. Henderson CR. Best Linear Unbiased Prediction of Nonadditive Genetic Merits in Noninbred Populations1. Journal of Animal Science. 1985; 60:111–117. Available from: http://dx.doi.org/10.2527/jas1985.601111x.

84. Rönnegård L, Pong-Wong R, Carlborg O. Defining the Assumptions Underlying Modeling of Epistatic QTL Using Variance Component Methods. Journal of Heredity. 2008 7; 99(4):421–425. Available from: http://jhered.oxfordjournals.org/content/99/4/421.abstract. https://doi.org/10.1093/jhered/esn017 PMID: 18344528

85. Chen H, Meigs JB, Dupuis J. Sequence Kernel Association Test for Quantitative Traits in Family Samples. Genetic epidemiology. 2013 2; 37(2):196–204. Available from: http://www.ncbi.nlm.nih.gov/pmc/articles/PMC3642218/. https://doi.org/10.1002/gepi.21703 PMID: 23280576

86. Kuonen D. Saddlepoint Approximations for Distributions of Quadratic Forms in Normal Variables. Biometrika. 1999; 86(4):929–935. Available from: http://www.jstor.org/stable/2673596. https://doi.org/10.1093/biomet/86.4.929

87. Satterthwaite FE. An Approximate Distribution of Estimates of Variance Components. Biometrics Bulletin. 1946; 2(6):110–114. Available from: http://www.jstor.org/stable/3002019. https://doi.org/10.2307/3002019 PMID: 20287815

88. The Wellcome Trust Case Control Consortium. Genome-wide association study of 14,000 cases of seven common diseases and 3,000 shared controls. Nature. 2007 6; 447(7145):661–678. Available from: http://dx.doi.org/10.1038/nature05911. PMID: 17554300

89. Wen X, Luca F, Pique-Regi R. Cross-Population Joint Analysis of eQTLs: Fine Mapping and Functional Annotation. PLoS Genet. 2015 4; 11(4):e1005176–. Available from: http://dx.doi.org/10.1371%2Fjournal.pgen.1005176. PMID: 25906321

90. Harrow J, Frankish A, Gonzalez JM, Tapanari E, Diekhans M, Kokocinski F, et al. GEN-CODE: The reference human genome annotation for The ENCODE Project. Genome Research. 2012 9; 22(9): 1760–1774. Available from: http://genome.cshlp.org/content/22/9/1760.abstract. https://doi.org/10.1101/gr.135350.111 PMID: 22955987

91. Stegle O, Parts L, Durbin R, Winn J. A Bayesian Framework to Account for Complex Non-Genetic Factors in Gene Expression Levels Greatly Increases Power in eQTL Studies. PLoS Comput Biol. 2010 5; 6(5):e1000770–. Available from: http://dx.doi.org/10.1371%2Fjournal.pcbi.1000770. PMID: 20463871

92. 1000 Genomes Project Consortium. An integrated map of genetic variation from 1,092 human genomes. Nature. 2012 11; 491(7422):56–65. Available from: http://dx.doi.org/10.1038/nature11632. PMID: 23128226

93. Pilia G, Chen WM, Scuteri A, Orrú M, Albai G, Dei M, et al. Heritability of Cardiovascular and Personality Traits in 6,148 Sardinians. PLoS Genet. 2006 8; 2(8):e132. Available from: http://dx.doi.org/10.1371%2Fjournal.pgen.0020132. PMID: 16934002

94. Huang Y, Wuchty S, Przytycka TM. eQTL Epistasis –Challenges and Computational Approaches. Frontiers in Genetics. 2013; 4:51. Available from: http://www.ncbi.nlm.nih.gov/pmc/articles/PMC3668133/. https://doi.org/10.3389/fgene.2013.00051 PMID: 23755066

95. Becker J, Wendland JR, Haenisch B, Nöthen MM, Schumacher J. A systematic eQTL study of cis—trans epistasis in 210 HapMap individuals. European Journal of Human Genetics. 2012 1; 20(1): 97–101. Available from: http://www.ncbi.nlm.nih.gov/pmc/articles/PMC3234520/. https://doi.org/10.1038/ejhg.2011.156 PMID: 21847142

96. Gamazon ER, Wheeler HE, Shah KP, Moza ari SV, Aquino-Michaels K, Carroll RJ, et al. A gene-based association method for mapping traits using reference transcriptome data. Nat Genet. 2015 9; 47(9):1091–1098. Available from: http://dx.doi.org/10.1038/ng.3367. PMID: 26258848

97. Young AI, Durbin R. Estimation of Epistatic Variance Components and Heritability in Founder Populations and Crosses. Genetics. 2014 12; 198(4):1405–1416. Available from: http://www.ncbi.nlm.nih.gov/pmc/articles/PMC4256760/. https://doi.org/10.1534/genetics.114.170795 PMID: 25326236

98. Lee SH, Wray NR, Goddard ME, Visscher PM. Estimating Missing Heritability for Disease from Genome-wide Association Studies. The American Journal of Human Genetics. 2011 2017/3/4; 88(3):294–305. Available from: http://dx.doi.org/10.1016/j.ajhg.2011.02.002.

99. Breslow NE, Clayton DG. Approximate Inference in Generalized Linear Mixed Models. Journal of the American Statistical Association. 1993; 88(421):9–25. Available from: http://www.jstor.org/stable/2290687. https://doi.org/10.1080/01621459.1993.10594284

100. Breslow NE, Lin X. Bias correction in generalised linear mixed models with a single component of dispersion. Biometrika. 1995 3; 82(1):81–91. Available from: http://dx.doi.org/10.1093/biomet/82.1.81.

101. Lin X, Breslow NE. Bias Correction in Generalized Linear Mixed Models With Multiple Components of Dispersion. Journal of the American Statistical Association. 1996; 91(435):1007–1016. Available from: http://www.jstor.org/stable/2291720. https://doi.org/10.1080/01621459.1996.10476971

102. Lin X. Variance component testing in generalised linear models with random effects. Biometrika. 1997 6; 84(2):309–326. Available from: http://biomet.oxfordjournals.org/content/84/2/309.abstract. https://doi.org/10.1093/biomet/84.2.309

103. Chen H, Wang C, Conomos MP, Stilp AM, Li Z, Sofer T, et al. Control for Population Structure and Relatedness for Binary Traits in Genetic Association Studies via Logistic Mixed Models. The American Journal of Human Genetics. 2016; 98(4):653–666. Available from: http://dx.doi.org/10.1016/j.ajhg.2016.02.012. PMID: 27018471

104. Lea AR, Tung J, Zhou X. A flexible, efficient binomial mixed model for identifying differential DNA methylation in bisulfite sequencing data. PLOS Genetics. 2015; 11:e1005650. https://doi.org/10.1371/journal.pgen.1005650 PMID: 26599596

105. Sun S, Hood M, Scott L, Peng Q, Mukherjee S, Tung J, et al. Differential expression analysis for RNA-seq using Poisson mixed models. Nucleic Acids Research. 2017; gkx204:gkx204.

106. Chernoff H, Lo SH, Zheng T. Discovering influential variables: A method of partitions. Ann Appl Stat. 2009; p. 1335–1369. Available from: http://projecteuclid.org/euclid.aoas/1267453943. https://doi.org/10.1214/09-AOAS265